© 2022. Published by The Company of Biologists Ltd | Journal of Cell Science (2022) 135, jcs259912. doi:10.1242/jcs.259912

RESEARCH ARTICLE

FCHSD2 is required for stereocilia maintenance in mouse cochlear hair cells

Xiaoyan Zhai[1], Haibo Du[1], Yuxin Shen[1], Xiujuan Zhang[1], Zhengjun Chen[2,3], Yanfei Wang[1] and Zhigang Xu[1,4,*]

ABSTRACT

Stereocilia are F-actin-based protrusions on the apical surface of inner-ear hair cells and are indispensable for hearing and balance perception. The stereocilia of each hair cell are organized into rows of increasing heights, forming a staircase-like pattern. The development and maintenance of stereocilia are tightly regulated, and deficits in these processes lead to stereocilia disorganization and hearing loss. Previously, we showed that the F-BAR protein FCHSD2 is localized along the stereocilia of cochlear hair cells and cooperates with CDC42 to regulate F-actin polymerization and cell protrusion formation in cultured COS-7 cells. In the present work, *Fchsd2* knockout mice were established to investigate the role of FCHSD2 in hearing. Our data show that stereocilia maintenance is severely affected in cochlear hair cells of *Fchsd2* knockout mice, which leads to progressive hearing loss. Moreover, *Fchsd2* knockout mice show increased acoustic vulnerability. Noise exposure causes robust stereocilia degeneration as well as enhanced hearing threshold elevation in *Fchsd2* knockout mice. Lastly, *Fchsd2*/*Cdc42* double knockout mice show more severe stereocilia deficits and hearing loss, suggesting that FCHSD2 and CDC42 cooperatively regulate stereocilia maintenance.

KEY WORDS: CDC42, FCHSD2, Hair cells, Hearing loss, Stereocilia

INTRODUCTION

Hair cells are the auditory and vestibular receptor cells in the inner ear. They are responsible for converting mechanical signals into electrical signals – a process that is known as mechano-electrical transduction (MET) (Fettiplace, 2017; Gillespie and Müller, 2009; Maoileidigh and Ricci, 2019). Hair cells are characterized by their hair bundles, which consist of dozens to hundreds of F-actin-based stereocilia and one microtubule-based kinocilium on the apical surface of each hair cell. Stereocilia are organized into several rows of increasing heights, forming a U-shaped or V-shaped staircase-like pattern. There are typically three rows of stereocilia in each mouse cochlear hair cell, usually referred to as the first (tall), second (middle) and third (short) rows. The kinocilium localizes at the vertex of each hair bundle, juxtaposed to the first-row stereocilia. The kinocilium plays important roles in hair bundle development but is not necessary for MET, and it is lost when cochlear hair cells mature (Hudspeth and Jacobs, 1979; Jones et al., 2008). In contrast, stereocilia play a pivotal role in MET (Hudspeth and Jacobs, 1979). Deflection of stereocilia towards the taller edge increases the open probability of MET channels at the tips of stereocilia in the shorter rows, which then leads to the MET currents (Beurg et al., 2009; Hudspeth and Jacobs, 1979).

The actin filaments in each stereocilium are interconnected by various actin crosslinkers – such as PLS1, FSCN2, ESPN and TRIOBP, among others (Kitajiri et al., 2010; Krey et al., 2016; Shin et al., 2010; Taylor et al., 2015; Zheng et al., 2000) – and are tightly packed into a paracrystalline array with barbed (plus) ends pointing towards the stereociliary tips (Flock and Cheung, 1977; Tilney et al., 1980). Stereocilia develop into the final mature structure in a multistep, precisely determined order by increasing the length and number of actin filaments (Krey et al., 2020; Tilney et al., 1992). In mature stereocilia, the F-actin core is quite stable, and actin monomer exchange only happens at the stereociliary tips (Drummond et al., 2015; Narayanan et al., 2015; Zhang et al., 2012). Consequently, stereocilia development and maintenance rely on the precise regulation of F-actin core assembly. The importance of stereociliary F-actin assembly is highlighted by the large number of deafness genes that encode actin or actin-regulatory proteins (Barr-Gillespie, 2015; Miyoshi et al., 2021).

The detailed mechanisms of stereocilia development and maintenance are being unraveled, and several proteins have been identified to play essential roles in these processes (Barr-Gillespie, 2015; Krey and Barr-Gillespie, 2019; Nayak et al., 2007; Vélez-Ortega and Frolenkov, 2019). One of these proteins is cell division cycle 42 (CDC42), a key regulator of the actin cytoskeleton. CDC42, Rac1 and RhoA belong to the Rho family of small GTPases and are all expressed in cochlear hair cells (Kalinec et al., 2000; Liu et al., 2014; Scheffer et al., 2015). CDC42 has been shown to stimulate ARP2/3-dependent actin polymerization in *Xenopus* egg extracts mainly through binding to actin nucleator N-WASP (also known as WASL; Rohatgi et al., 1999). Previously, we and others have shown that CDC42 is localized in cochlear hair cell stereocilia, and that *Cdc42* gene knockout affects stereocilia development and maintenance in mice (Du et al., 2021; Kirjavainen et al., 2015; Ueyama et al., 2014).

FCH domain and double SH3 domains-containing protein 2 (FCHSD2) is a member of the FCH and Bin-Amphiphysin-Rvs (F-BAR) protein family, which consists of cytosolic proteins that regulate actin polymerization, membrane curvature and cell motility (Carman and Dominguez, 2018; Salzer et al., 2017). Previously, we showed that FCHSD2 is localized along the hair cell stereocilia and is able to stimulate WASP–ARP2/3-mediated actin polymerization *in vitro*, suggesting that FCHSD2 might play a role in stereocilia development and/or maintenance (Cao et al., 2013). Recently,

[1]Shandong Provincial Key Laboratory of Animal Cell and Developmental Biology and Key Laboratory for Experimental Teratology of the Ministry of Education, School of Life Sciences, Shandong University, Qingdao, Shandong 266237, China. [2]State Key Laboratory of Cell Biology, Shanghai Institute of Biochemistry and Cell Biology, Center for Excellence in Molecular Cell Science, Chinese Academy of Sciences (CAS), Shanghai 200031, China. [3]School of Life Science and Technology, ShanghaiTech University, Shanghai 200031, China. [4]Shandong Provincial Collaborative Innovation Center of Cell Biology, Shandong Normal University, Jinan, Shandong 250014, China.

*Author for correspondence (xuzg@sdu.edu.cn)

X. Zhai, 0000-0002-3657-1994; Z.X., 0000-0003-0082-7297

Handling Editor: Michael Way
Received 11 February 2022; Accepted 15 July 2022

Journal of Cell Science (2022) 135, jcs259912. doi:10.1242/jcs.259912

we reported that FCHSD2 cooperates with CDC42 and N-WASP to regulate cell protrusion formation in COS-7 cells (Zhai et al., 2022). In the present work, we establish two *Fchsd2* knockout mouse lines and show that loss of FCHSD2 leads to deficits in stereocilia maintenance as well as hearing loss. Furthermore, *Fchsd2*/*Cdc42* double knockout mice show more severe stereocilia deficits and hearing loss, suggesting that FCHSD2 and CDC42 might cooperatively regulate stereocilia maintenance in mice.

RESULTS

Fchsd2 knockout mice show progressive hearing loss

The mouse *Fchsd2* gene has 21 exons – with the translational start codon localized in exon 1 and the translational stop codon localized in exon 21 – and encodes a protein of 749 amino acids. Exon 11 is subjected to alternative splicing, which gives rise to two FCHSD2 isoforms with or without an insertion of 24 amino acids (NP_950177.2 and NP_001139482.1). We introduced two *loxP* sequences on each side of exon 2 through homologous recombination and obtained $Fchsd2^{loxP/+}$ mice (Fig. 1A). By crossing $Fchsd2^{loxP/+}$ mice with $EIIa\text{-}Cre^{+/-}$ transgenic mice, we obtained $EIIa\text{-}Cre^{+/-}$; $Fchsd2^{loxP/loxP}$ mice, in which exon 2 of the *Fchsd2* gene is ubiquitously deleted in all somatic and germline cells (Fig. 1A). Thereafter, all of the homozygous offspring of these mice have exon 2 of the *Fchsd2* gene deleted and are therefore referred to as $Fchsd2^{-/-}$ in the following text. Exon 2 consists of 98 bp, and its deletion causes a premature translational stop in the *Fchsd2* transcript. Western blotting using a custom antibody raised against amino acids 1–631 of mouse FCHSD2 was employed to examine the expression of FCHSD2 in $Fchsd2^{-/-}$ mice. The predicted molecular mass of mouse FCHSD2 is 84.3 kDa. A band with a molecular mass of ∼90 kDa was detected in all the tissues examined of wild-type and $Fchsd2^{+/-}$ mice, including the inner ear, but this band was not detected in $Fchsd2^{-/-}$ mice (Fig. 1B). Several additional weak bands were also detected, which might result from unspecific binding of the antibody (Fig. 1B). Furthermore, whole-mount immunostaining of cochlear sensory epithelia showed that FCHSD2 immunoreactivity is localized on the perimeter of the stereociliary F-actin core in $Fchsd2^{+/-}$ mice, but not in $Fchsd2^{-/-}$ mice (Fig. 1C–C″). Taken together, the western blot and immunostaining results confirm that $Fchsd2^{-/-}$ mice are devoid of FCHSD2 protein in the inner ear.

The $Fchsd2^{-/-}$ mice were found to be morphologically and behaviorally indistinguishable from $Fchsd2^{+/-}$ or wild-type mice. Furthermore, interbreeding of $Fchsd2^{+/-}$ mice gave rise to offspring in the expected Mendelian ratio (25% wild type, 47.7% $Fchsd2^{+/-}$ and 27.3% $Fchsd2^{-/-}$; n=44; P=0.967; χ^2 test) with normal viability, and both male and female $Fchsd2^{-/-}$ mice were found to be fertile. These results suggest that FCHSD2 is dispensable for general development and reproduction in mice. Auditory brainstem response (ABR) measurements were then performed to evaluate the auditory function of $Fchsd2^{-/-}$ mice. When examined at age of 1 month or 2 months, the ABR thresholds of $Fchsd2^{-/-}$ mice to click stimuli were not significantly different from those of $Fchsd2^{+/-}$ mice (Fig. 1D). However, a 20 decibels (dB) ABR threshold elevation was observed in $Fchsd2^{-/-}$ mice at an age of 3 months (Fig. 1D). The hearing threshold elevation of $Fchsd2^{-/-}$ mice reached 40 dB at an age of 9 months, and $Fchsd2^{-/-}$ mice were profoundly deaf, with a hearing threshold above 90 dB sound pressure level (SPL), by 12 months of age (Fig. 1D). Moreover, our data show that ABR thresholds of $Fchsd2^{-/-}$ mice to pure-tone stimuli are elevated in all frequencies when examined at an age of 5 months (Fig. 1F). Taken together, the ABR measurements suggest that $Fchsd2^{-/-}$ mice suffer progressive hearing loss. Our present data also reveal that the hearing thresholds are not significantly different between $Fchsd2^{+/-}$ mice and $Fchsd2^{+/+}$ mice (Fig. 1E), therefore $Fchsd2^{+/-}$ mice were used as controls in the following work.

We also established another *Fchsd2* knockout mouse line using the clustered regularly interspaced short palindromic repeat (CRISPR)-associated Cas9 nuclease (CRISPR/Cas9) genome editing technique. A deletion of 37 bp was introduced into exon 2, which causes a frameshift and premature translational stop in the *Fchsd2* gene (Fig. S1A). The resulting mouse line is referred to as $Fchsd2^{+/\Delta 37}$ hereafter. Western blotting and whole-mount immunostaining confirmed that FCHSD2 protein is absent in $Fchsd2^{\Delta 37/\Delta 37}$ mice (Fig. S1B and data not shown). Consistent with the results obtained from $Fchsd2^{-/-}$ mice, $Fchsd2^{\Delta 37/\Delta 37}$ mice were found to be developmentally normal but manifest progressive hearing loss (Fig. S1C,D).

Stereocilia maintenance is affected in *Fchsd2* knockout mice

Scanning electron microscopy (SEM) was performed to examine the morphology of hair cell stereocilia in the *Fchsd2* knockout mice. Stereocilia of both inner hair cells (IHCs) and outer hair cells (OHCs) in 1-month-old $Fchsd2^{-/-}$ mice were found to have intact stereocilia similar to those of $Fchsd2^{+/-}$ control mice (Fig. S2). At an age of 2 months, however, complete stereocilia loss could be observed in some $Fchsd2^{-/-}$ OHCs at the basal turn (Fig. 2A,C). Complete OHC stereocilia loss became more severe in 3-month-old $Fchsd2^{-/-}$ cochlea and extended from the basal to the middle turn (Fig. 2B,C). Meanwhile, IHC stereocilia were found to largely remain intact in $Fchsd2^{-/-}$ cochlea (Fig. 2A,B,D).

Hair cell survival was then examined by performing whole-mount immunostaining using an antibody against the hair cell marker myosin VIIA (MYO7A) (Hasson et al., 1997). There was no obvious hair cell loss in $Fchsd2^{-/-}$ mice at 1 month, but significant OHC loss was observed by an age of 3 months at the basal and middle turns in $Fchsd2^{-/-}$ mice (Fig. 2E,F). The percentage of OHC loss was ∼36% at the basal turn of 3-month-old $Fchsd2^{-/-}$ mice, compared to 4% in age-matched control $Fchsd2^{+/-}$ mice. By an age of 5 months, OHC loss became more severe in $Fchsd2^{-/-}$ mice, whereas IHCs were still largely unaffected at this age (Fig. 2E,F).

We then used SEM imaging to examine the stereocilia in more detail. By an age of 2 months, degeneration of third-row stereocilia could be observed in some OHCs at middle and basal turns (Fig. 3A,C). The third-row stereocilia degeneration became more severe and extended to all the three turns by 3 months of age (Fig. 3B,C). Meanwhile, IHC stereocilia remained intact in both 2-month-old and 3-month-old $Fchsd2^{-/-}$ mice (Fig. 3A,B). Similar phenotypes were observed in $Fchsd2^{\Delta 37/\Delta 37}$ mice (Fig. S1E–H). We also measured the length of first-row stereocilia in IHCs and OHCs, which did not reveal any significant difference between 3-month-old $Fchsd2^{-/-}$ and $Fchsd2^{+/-}$ mice (Fig. 3D). Taken together, our data suggest that knockout of *Fchsd2* affects stereocilia maintenance in OHCs.

Fchsd2 knockout mice show increased acoustic vulnerability

It has been shown that stereocilia deficits are associated with noise-induced hearing loss (Avinash et al., 1993; Engström et al., 1983; Liberman, 1987; Liberman and Dodds, 1987; Tilney et al., 1982). We examined whether *Fchsd2* knockout mice are more vulnerable to noise insults. $Fchsd2^{-/-}$ and $Fchsd2^{+/-}$ mice at an

Journal of Cell Science (2022) 135, jcs259912. doi:10.1242/jcs.259912

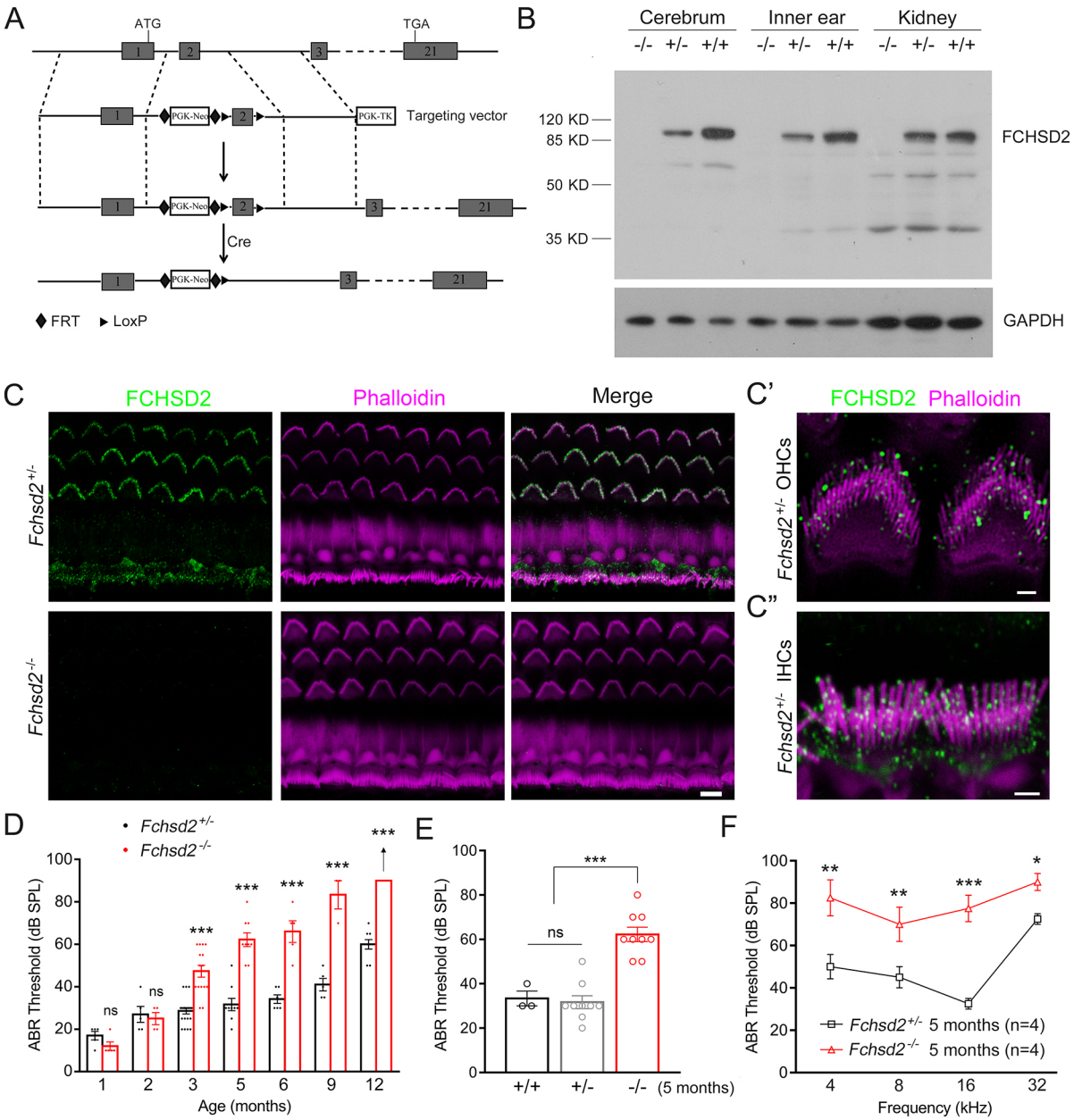

Fig. 1. *Fchsd2*$^{-/-}$ mice show progressive hearing loss. (A) Schematic drawing of the strategy for constructing *Fchsd2*$^{-/-}$ mice. The targeting vector has two *loxP* sites flanking exon 2 of the *Fchsd2* gene. After successful homologous recombination, the *loxP* sites were placed at both sides of exon 2 of the *Fchsd2* gene in the mouse genome. With the help of Cre recombinase, exon 2 is excised, resulting in disruption of the *Fchsd2* gene. Exons are marked as numbered boxes; PGK-Neo and PGK-TK represent resistance genes used for selection (see Materials and Methods); FRT, flippase recognition target. (B) Expression of FCHSD2 in various tissues from 1-month-old mice of *Fchsd2*$^{-/-}$, *Fchsd2*$^{+/-}$ and *Fchsd2*$^{+/+}$ genotypes, as indicated, was examined by western blotting using an anti-FCHSD2 antibody. GAPDH was used as internal control. Molecular mass is indicated in kDa (KD). Blots shown are representative of three experiments. (C) Expression of FCHSD2 in the stereocilia of postnatal day 21 *Fchsd2*$^{+/-}$ and *Fchsd2*$^{-/-}$ mice was examined by performing whole-mount immunostaining using an anti-FCHSD2 antibody. The F-actin cores of stereocilia were visualized using TRITC-conjugated phalloidin. Images were taken using a confocal microscope. Scale bar: 5 µm. (C′) Higher magnification image showing FCHSD2 immunoreactivity and phalloidin staining in the stereocilia of postnatal day 28 (P28) *Fchsd2*$^{+/-}$ OHCs. Scale bar: 1 µm. (C″) Higher magnification image showing FCHSD2 immunoreactivity and phalloidin staining in the stereocilia of P28 *Fchsd2*$^{+/-}$ IHCs. Scale bar: 2 µm. Images in C–C″ are representative of three experiments. (D) ABR thresholds to click stimuli in *Fchsd2*$^{+/-}$ and *Fchsd2*$^{-/-}$ mice at different ages. Arrow indicates threshold above 90 dB SPL. Each dot represents an individual mouse. (E) ABR thresholds to click stimuli in 5-month-old *Fchsd2*$^{+/+}$, *Fchsd2*$^{+/-}$ and *Fchsd2*$^{-/-}$ mice. Each circle represents an individual mouse. (F) ABR thresholds to pure tone stimuli in 5-month-old *Fchsd2*$^{+/-}$ and *Fchsd2*$^{-/-}$ mice. The numbers of animals used for each genotype are indicated in brackets. Data in D–F are presented as mean±s.e.m. **P*<0.05; ***P*<0.01; ****P*<0.001; ns, not significant (one-way ANOVA with Tukey's test).

age of 1 month were exposed to a broadband noise of 2–20 kHz at 106 dB SPL for 2 h, and the ABR thresholds were measured at different time points before and after the noise exposure (Fig. 4A). Similar protocols have been shown to induce a slight or moderate permanent threshold shift (PTS) at 2 weeks after noise exposure in mice (Chen et al., 2012; Gong et al., 2012). During the experiment, some of the mice were euthanized, and the stereocilia and ribbon synapses were examined using SEM and immunostaining at certain time points (Fig. 4A). ABR measurements show that the noise exposure induced a slight PTS in control *Fchsd2*$^{+/-}$

Journal of Cell Science (2022) 135, jcs259912. doi:10.1242/jcs.259912

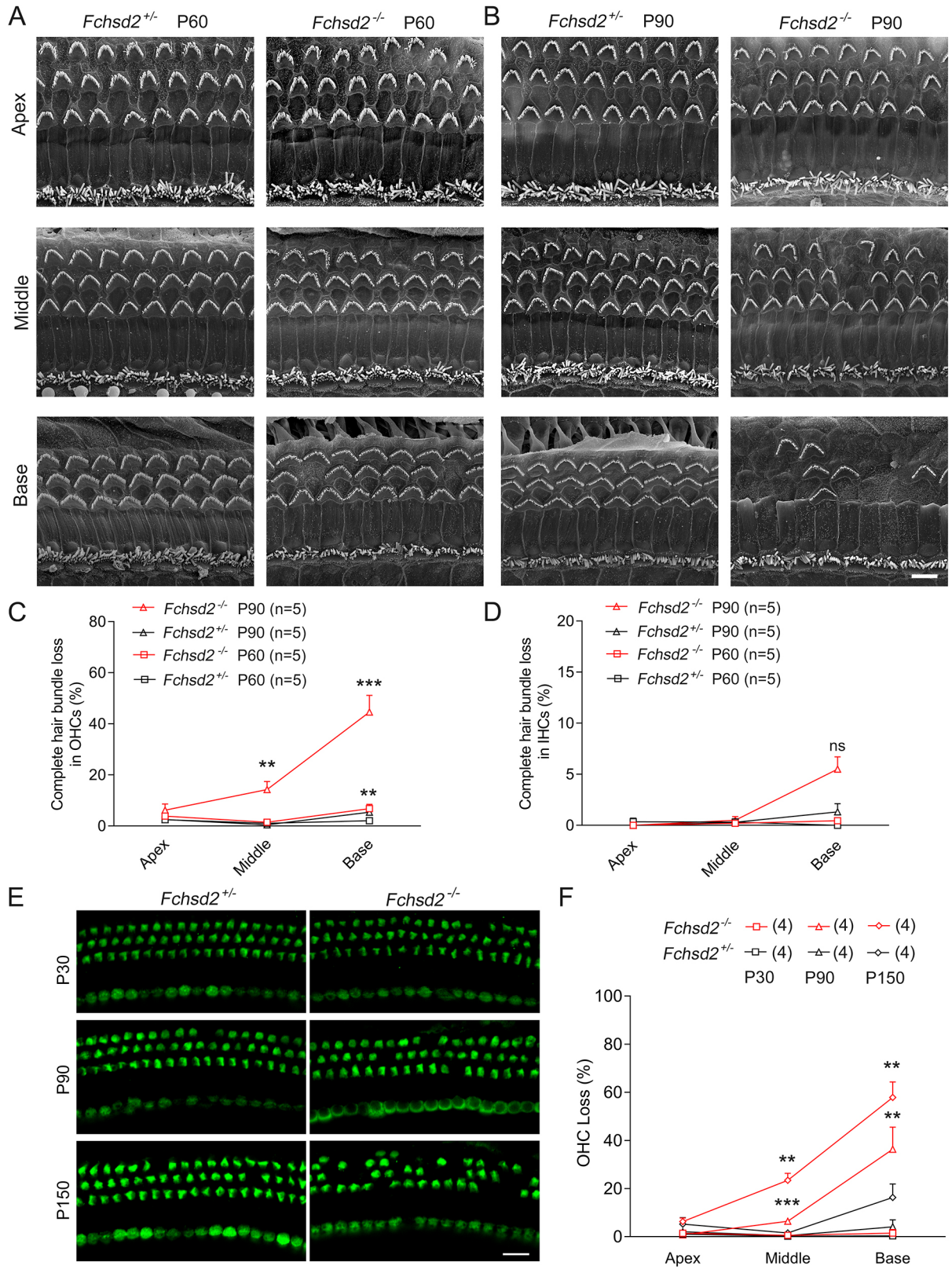

Fig. 2. Stereocilia maintenance and OHC survival are affected in *Fchsd2*$^{-/-}$ mice. (A,B) SEM images of hair bundles at the apical (apex), middle and basal (base) turns of the cochlea of *Fchsd2*$^{+/-}$ and *Fchsd2*$^{-/-}$ mice at (A) postnatal day 60 (P60) and (B) postnatal day 90 (P90). Scale bar: 5 µm. (C) Percentage of complete OHC hair bundle loss, calculated based on images as shown in A and B. (D) Percentage of complete IHC hair bundle loss, calculated based on images as shown in A and B. (E) Immunostaining was performed using an anti-MYO7A antibody at postnatal day 30 (P30), P90 and postnatal day 150 (P150). Shown are single confocal images of the basal-middle turn (i.e. the basal turn that is adjacent to the middle turn) of cochlea from mice of the indicated genotypes. Scale bar: 10 µm. (F) OHC loss quantified according to the results from E. Data in C,D,F are presented as mean+s.e.m. Numbers of mice used in each group are indicated in brackets. ***P*<0.01; ****P*<0.001; ns, not significant (one-way ANOVA with Dunnett's test).

Journal of Cell Science (2022) 135, jcs259912. doi:10.1242/jcs.259912

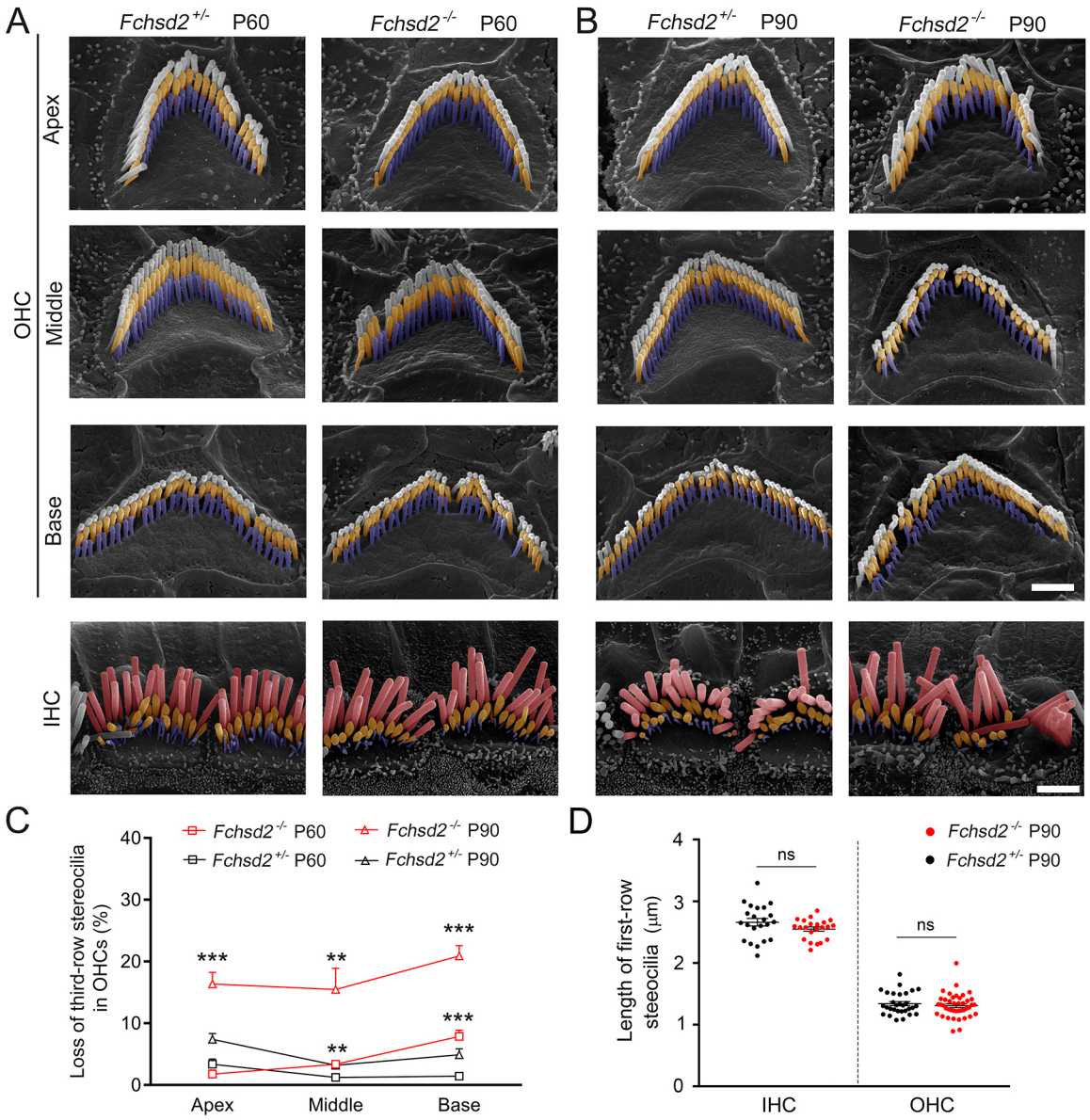

Fig. 3. Degeneration of third-row stereocilia in *Fchsd2*$^{-/-}$ OHCs. (A,B) Cochlear hair cell stereocilia of *Fchsd2*$^{+/-}$ and *Fchsd2*$^{-/-}$ mice at (A) postnatal day 60 (P60) or (B) postnatal day 90 (P90) were analyzed by SEM. Top panels, higher magnification SEM images of OHCs at different turns, as indicated. Scale bar: 1 µm (applies to both A and B). Bottom panel, higher magnification SEM images of IHCs at middle turn. Scale bar: 2 µm (applies to both A and B). First-row stereocilia are shown in red in IHCs and are not colored in OHCs; second-row stereocilia are shown in yellow; third-row stereocilia are shown in violet. (C) Percentages of third-row stereocilia loss in OHCs, as calculated using the SEM results. For each group, at least 30 cells from at least three mice were analyzed. Data are presented as mean+s.e.m. (D) Length of first-row stereocilia in middle-turn IHCs or OHCs, as measured in SEM images. For each group, at least 22 stereocilia from five cells of three mice were analyzed. Data are presented as mean±s.e.m. ***P*<0.01; ****P*<0.001; ns, not significant (one-way ANOVA with Dunnett's test in C; two-tailed paired Student's *t*-test in D).

mice (Fig. 4B). However, the same noise exposure induced significantly increased PTS in *Fchsd2*$^{-/-}$ mice, suggesting that *Fchsd2*$^{-/-}$ mice are more vulnerable to noise insults (Fig. 4B).

SEM analysis revealed that at 2 h after noise exposure, the stereocilia morphology was largely normal in *Fchsd2*$^{-/-}$ mice (Fig. 4C). However, significant OHC stereocilia loss at middle and basal turns was observed in *Fchsd2*$^{-/-}$ mice at 4 days after noise, which became more severe at 14 days after noise (Fig. 4C,D). Meanwhile, IHC stereocilia in *Fchsd2*$^{-/-}$ mice largely remained intact at all the time points examined (Fig. 4C). As a control, stereocilia in both OHCs and IHCs were largely unaffected by the noise in *Fchsd2*$^{+/-}$ mice (Fig. 4C,D). Consistently, phalloidin and DAPI staining showed that loss of OHCs, but not of IHCs, occurred at 4 days after noise exposure in *Fchsd2*$^{-/-}$ mice, and this loss was exaggerated at 14 days after exposure to noise (Fig. 4E; Fig. S3).

High-magnification SEM imaging was then used to examine the stereocilia in more detail. Increased third-row stereocilia degeneration was detected in OHCs of *Fchsd2*$^{-/-}$ mice at 2 h after noise exposure, especially at the basal turn, and this degeneration became more severe at 4 and 14 days after noise exposure (Fig. 5A,D). Meanwhile, first-row stereocilia degeneration was also observed in *Fchsd2*$^{-/-}$ OHCs following noise exposure (Fig. 5A,C). IHCs of *Fchsd2*$^{-/-}$ mice were found to be largely unaffected (Fig. 5B). Taken together, our data suggest that exposure to noise causes robust OHC stereocilia degeneration, which

Journal of Cell Science (2022) 135, jcs259912. doi:10.1242/jcs.259912

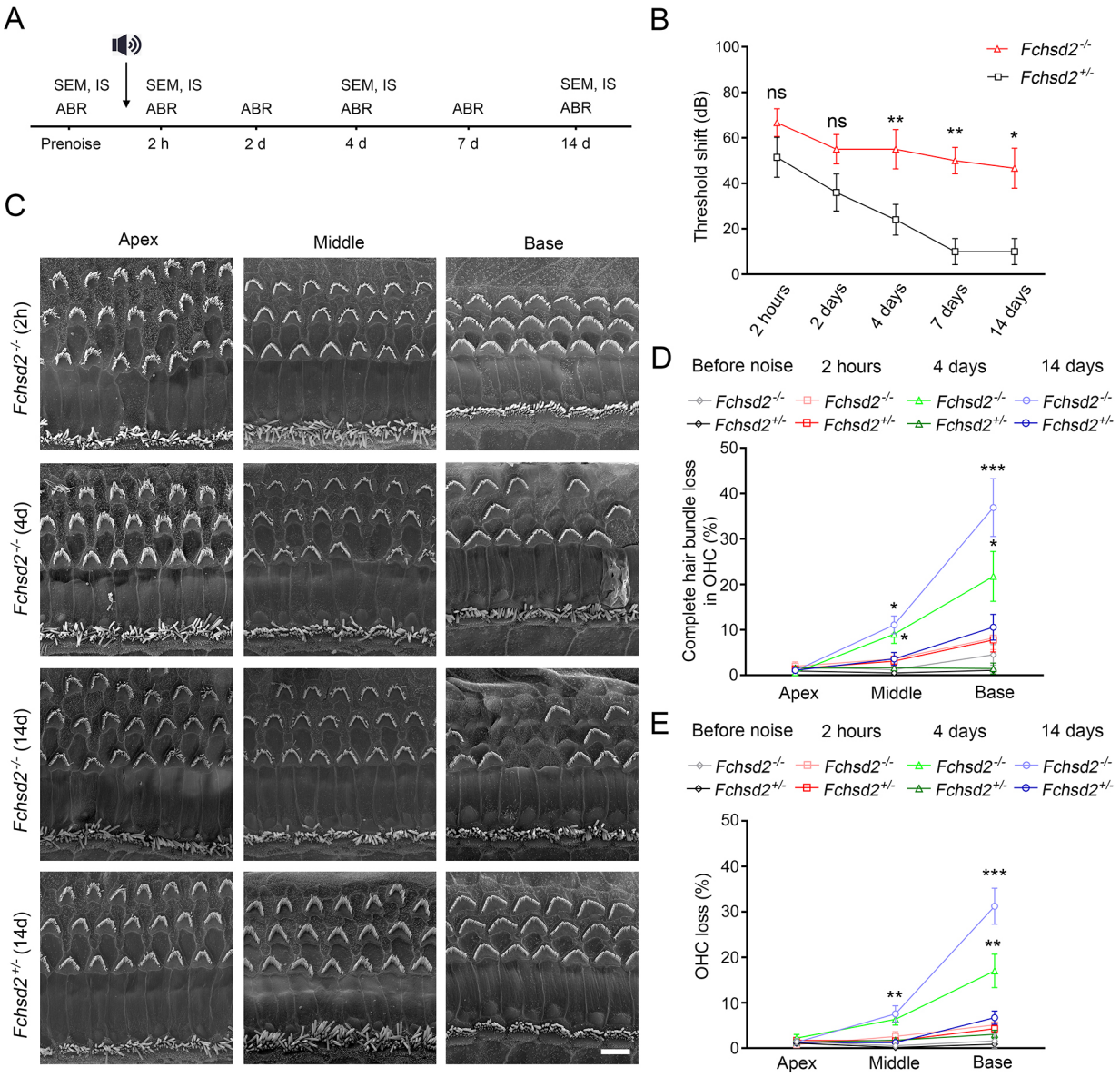

Fig. 4. *Fchsd2* knockout mice show increased acoustic vulnerability. (A) Schematic drawing of the strategy for the noise exposure experiment. *Fchsd2*$^{+/-}$ and *Fchsd2*$^{-/-}$ mice at 1 month were exposed to a broadband noise of 2–20 kHz at 106 dB SPL for 2 h, and the ABR thresholds were measured at different time points, as indicated. At certain time points, some of the mice were euthanized and the stereocilia and ribbon synapses were examined using SEM and immunostaining (IS). (B) ABR threshold shift in responses to click stimuli for mice of the indicated genotypes at different time points following noise exposure. (C) SEM images of hair bundles at the apical (apex), middle and basal (base) turns in *Fchsd2*$^{+/-}$ and *Fchsd2*$^{-/-}$ mice at different time points following noise exposure, as indicated. Scale bar: 5 µm. (D) Percentage of complete OHC hair bundle loss at different positions following noise exposure, quantified using SEM images as shown in C. (E) Percentage of OHC loss at different positions following noise exposure, quantified using the immunostaining results from Fig. S3. Data in B,D,E are presented as mean±s.e.m., and at least three mice were used per group. *P<0.05; **P<0.01; ***P<0.001; ns, not significant (one-way ANOVA with LSD test in B; one-way ANOVA with Dunnett's test in D,E).

may eventually lead to increased OHC loss and hearing threshold elevation in *Fchsd2* knockout mice.

Loss of IHC ribbon synapses has been suggested to be associated with noise-induced hearing loss (Kobel et al., 2017; Kujawa and Liberman, 2009; Liberman, 2017). We examined the ribbon synapses by performing whole-mount immunostaining using antibodies to detect CtBP2 and GluR2 (also known as GRIA2). The results showed that in control mice, the numbers of double-positive ribbon synapses decreased at 2 h after noise but recovered to the normal level by 14 days after noise exposure (Fig. S4). Interestingly, similar recovery of IHC ribbon synapses was observed in *Fchsd2*$^{-/-}$ mice (Fig. S4), suggesting that ribbon synapse deficits do not contribute to the severe PTS observed in *Fchsd2*$^{-/-}$ mice.

Fchsd2/*Cdc42* double knockout mice show more severe stereocilia deficits and hearing loss

Nervous wreck (Nwk), the *Drosophila* homolog of FCHSD2, shares 41% amino acid identity for the F-BAR domain and 54% amino acid identity for the SH3 domains with FCHSD2 (Cao et al., 2013). It has been shown that Nwk cooperates with Cdc42 to regulate actin polymerization and synaptic growth (Rodal et al., 2008). Nwk and Cdc42 colocalize in periactive zones of the neuromuscular junction, and *cdc42*; *nwk* double mutants show an

Journal of Cell Science (2022) 135, jcs259912. doi:10.1242/jcs.259912

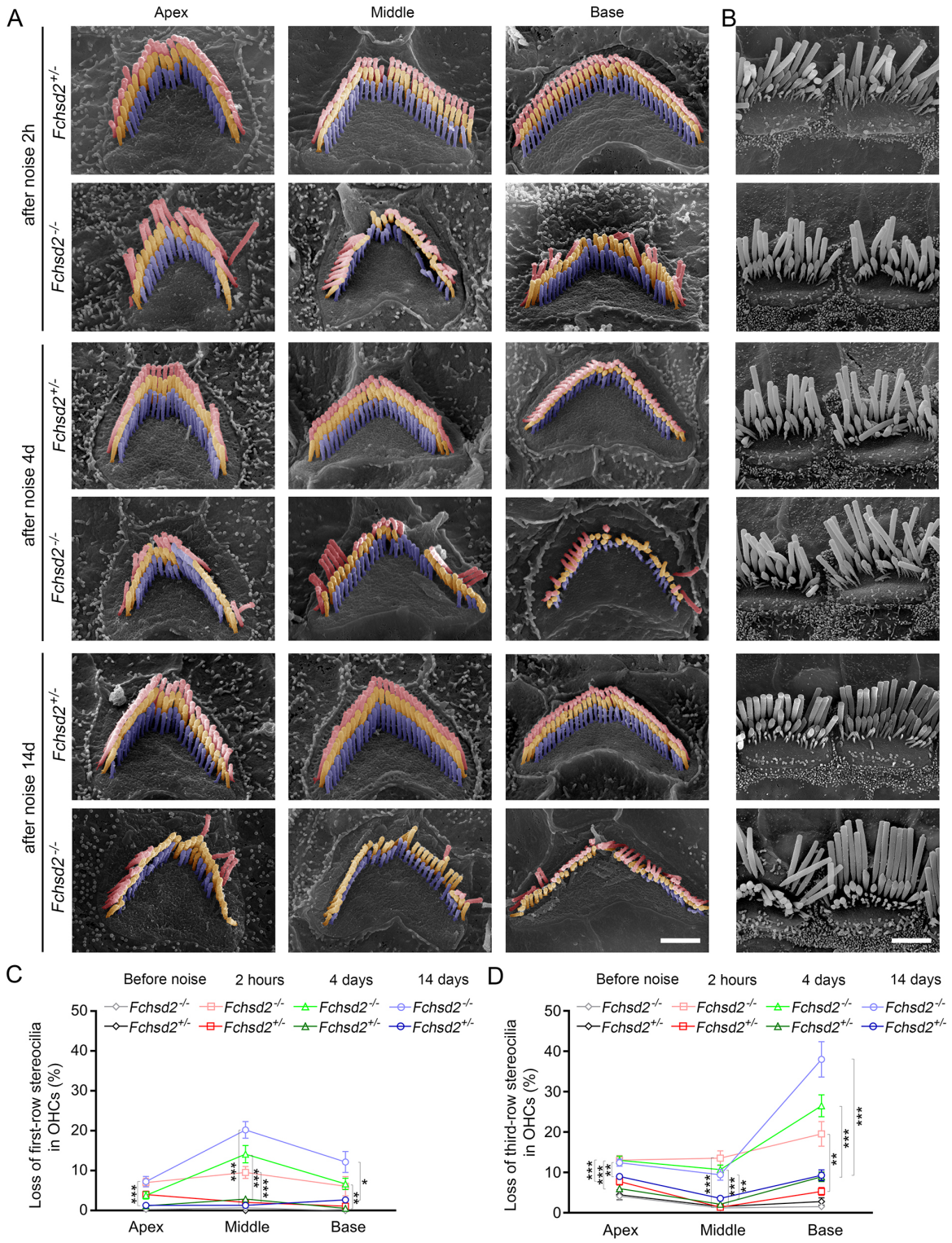

Fig. 5. Noise-induced stereocilia degeneration is enhanced in *Fchsd2* knockout mice. (A) Higher magnification SEM images of OHCs at the apical (apex), middle and basal (base) turns for the indicated genotypes and time points after noise exposure. First-row stereocilia are shown in red; second-row stereocilia are shown in yellow; third-row stereocilia are shown in violet. Scale bar: 1 µm. (B) Higher magnification SEM images of IHCs at middle turn for the genotypes and time points indicated in A. Scale bar: 2 µm. (C) Percentage of first-row stereocilia loss in OHCs, calculated using images as shown in A. (D) Percentage of third-row stereocilia loss in OHCs, calculated using images as shown in A. Data in C and D are presented as mean±s.e.m. For each group, at least 40 cells from at least three mice were analyzed. **P*<0.05; ***P*<0.01; ****P*<0.001; ns, not significant (one-way ANOVA with Dunnett's test).

additive effect on synaptic growth (Rodal et al., 2008). Moreover, FCHSD2 cooperates with CDC42 to regulate cell protrusion formation in COS-7 cells (Zhai et al., 2022). CDC42 has been shown to localize in the stereocilia, and *Cdc42* knockout in mouse leads to stereocilia deficits such as third-row stereocilia degeneration, extra fourth-row stereocilia, as well as dysregulated

Journal of Cell Science (2022) 135, jcs259912. doi:10.1242/jcs.259912

planer cell polarity (Du et al., 2021; Kirjavainen et al., 2015; Ueyama et al., 2014). Therefore, we next examined whether FCHSD2 and CDC42 could cooperate in mammalian hair cells by evaluating the auditory function of the corresponding knockout mice. By an age of 1 month, when *Fchsd2*$^{-/-}$ mice still show normal ABR threshold, *Atoh1-Cre*$^{+/-}$; *Cdc42*$^{loxP/loxP}$ mice exhibited a 20 dB threshold elevation to click stimuli (Fig. 6A). Interestingly, loss of one copy of the *Cdc42* gene in a *Fchsd2*$^{-/-}$ background or loss of one copy of the *Fchsd2* gene in an *Atoh1-Cre*$^{+/-}$; *Cdc42*$^{loxP/loxP}$ background resulted in threshold elevation of 30 and 40 dB, respectively (Fig. 6A). Furthermore, *Atoh1-Cre*$^{+/-}$; *Cdc42*$^{loxP/loxP}$; *Fchsd2*$^{-/-}$ double knockout mice showed the highest threshold elevation, which was nearly 60 dB (Fig. 6A). The hearing thresholds of knockout mice were further elevated at an age of 2 months (Fig. S5). These results suggest that FCHSD2 and CDC42 cooperate to regulate auditory function in mice.

SEM was then employed to examine the cooperative role of FCHSD2 and CDC42 in stereocilia maintenance. At an age of 1 month, *Cdc42*$^{loxP/loxP}$ and *Cdc42*$^{loxP/loxP}$; *Fchsd2*$^{-/-}$ mice were found to have intact stereocilia, whereas *Atoh1-Cre*$^{+/-}$; *Cdc42*$^{loxP/loxP}$ mice exhibited significant OHC stereocilia loss (Fig. 6B,C). Loss of one copy of the *Cdc42* gene in a *Fchsd2*$^{-/-}$ background or vice versa resulted in more robust OHC stereocilia loss, whereas *Atoh1-Cre*$^{+/-}$; *Cdc42*$^{loxP/loxP}$; *Fchsd2*$^{-/-}$ double knockout mice showed the most severe OHC stereocilia loss (Fig. 6B,C). Our data reveal that *Cdc42* knockout also affects IHC stereocilia maintenance, and we found that this effect is exaggerated by *Fchsd2* knockout (Fig. 6B,D). Consistently, more robust hair cell loss was observed in *Atoh1-Cre*$^{+/-}$; *Cdc42*$^{loxP/loxP}$; *Fchsd2*$^{-/-}$ double knockout mice than in each single knockout mouse line (Fig. 7A–C).

We then examined the detailed stereocilia morphology of double knockout mice at an age of 1 month using higher magnification SEM. In *Cdc42*$^{loxP/loxP}$; *Fchsd2*$^{-/-}$ mice, OHC stereocilia were found to be nicely organized into three rows of increasing heights, similarly to those of *Fchsd2*$^{-/-}$ mice (Fig. S2B) and *Cdc42*$^{loxP/loxP}$ mice (Fig. 8A). However, sporadic degeneration of individual third-row stereocilia was observed in *Atoh1-Cre*$^{+/-}$; *Cdc42*$^{loxP/loxP}$ OHCs (Fig. 8A,C). OHC stereocilia degeneration was exaggerated in *Atoh1-Cre*$^{+/-}$; *Cdc42*$^{loxP/loxP}$; *Fchsd2*$^{+/-}$ OHCs as well as in *Atoh1-Cre*$^{+/-}$; *Cdc42*$^{loxP/+}$; *Fchsd2*$^{-/-}$ OHCs, and the most robust stereocilia degeneration was observed in *Atoh1-Cre*$^{+/-}$; *Cdc42*$^{loxP/loxP}$; *Fchsd2*$^{-/-}$ OHCs (Fig. 8A,C). Stereocilia fusion could be observed in some *Atoh1-Cre*$^{+/-}$; *Cdc42*$^{loxP/loxP}$ IHCs, and this fusion was exacerbated in *Atoh1-Cre*$^{+/-}$; *Cdc42*$^{loxP/loxP}$; *Fchsd2*$^{-/-}$ IHCs (Fig. 8B). Taken together, our data suggest that FCHSD2 and CDC42 cooperate to regulate stereocilia maintenance and auditory function in mice.

DISCUSSION

Stereocilia development and maintenance rely on the precise regulation of F-actin core assembly. With genetic and proteomic advances, many proteins have been identified to play essential roles in this process (Barr-Gillespie, 2015; Krey and Barr-Gillespie, 2019; Nayak et al., 2007; Vélez-Ortega and Frolenkov, 2019). Previously, we have shown that FCHSD2 is localized along the stereocilia of auditory hair cells and is able to promote cell protrusion formation in cultured cells, suggesting that it might play a role in stereocilia development and/or maintenance (Cao et al., 2013; Zhai et al., 2022). In the present work, we established *Fchsd2* knockout mice and showed that FCHSD2 is indispensable for stereocilia maintenance. As a result, *Fchsd2* knockout mice suffer from progressive hearing loss.

FCHSD2 is a member of the BAR protein superfamily, which is characterized by the presence of the BAR domain that promotes membrane curvature in antiparallel homodimers (Peter et al., 2004; Simunovic et al., 2019). BAR proteins are categorized into three major subfamilies, namely N-BAR, F-BAR and I-BAR proteins, according to the sequence homology and structure similarity of the BAR domains (Carman and Dominguez, 2018). The classical crescent N-BAR domain and the more extended and less curved F-BAR domain usually promote membrane invaginations, whereas the inverse curvature I-BAR domain usually generates membrane protrusions (Carman and Dominguez, 2018). FCHSD2 has long been considered to be an F-BAR protein. Evidence from others and our group show that overexpression of the FCHSD2 F-BAR domain promotes formation of plasma membrane protrusions in cultured cells (Almeida-Souza et al., 2018; Becalska et al., 2013; Kelley et al., 2015; Zhai et al., 2022). Our present work shows that FCHSD2 is indispensable for the maintenance of stereocilia, a special type of actin-based, microvilli-like cell protrusions in inner-ear hair cells, further supporting that FCHSD2 behaves as an atypical F-BAR protein. A similar scenario has been reported for SRGAP1, SRGAP2 and SRGAP3, whose F-BAR domains induce cell protrusions in cultured cells and are therefore referred to as inverse F-BAR (IF-BAR) domains (Carlson and Soderling, 2009; Carlson et al., 2011; Coutinho-Budd et al., 2012; Guerrier et al., 2009). Our results suggest that FCHSD2 could be considered as another member of the IF-BAR protein subfamily.

In *Fchsd2* knockout mice, stereocilia were intact in both OHCs and IHCs when examined at an age of 1 month. Stereocilia degeneration was first observed in OHCs of 2-month-old *Fchsd2* knockout mice, when hearing impairment had not yet manifested. Noticeably, we found that stereocilia degeneration in *Fchsd2* knockout OHCs is mostly limited to the third-row stereocilia, leaving the first- and second-row stereocilia largely unaffected. The degeneration of the mechanosensitive third-row stereocilia might affect the MET function of OHCs. Complete OHC stereocilia loss as well as OHC loss became apparent by an age of 3 months, which is consistent with the progressive hearing loss observed in *Fchsd2* knockout mice. Mice lacking EPS8L2, MYO15A-L (the long isoform of MYO15A), BAIAP2L2 or PJVK have been reported to show similar third-row stereocilia degeneration in both OHCs and IHCs (Carlton et al., 2021; Fang et al., 2015; Furness et al., 2013; Kazmierczak et al., 2017; Yan et al., 2022). Different from the ubiquitous expression pattern of FCHSD2 along the stereocilia, EPS8L2, MYO15A-L and BAIAP2L2 are localized at the tips of shorter-row stereocilia, whereas PJVK is suggested to mainly localize at the stereociliary rootlet (Carlton et al., 2021; Fang et al., 2015; Furness et al., 2013; Kazmierczak et al., 2017; Yan et al., 2022). It awaits further investigation whether FCHSD2 could functionally interact with these proteins to regulate stereocilia maintenance.

Stereocilia damage has been known as a hallmark of permanent noise-induced hearing loss for decades (Liberman, 1987). Noise exposure can induce stereocilia deficits ranging from stereocilia degeneration and fusion to rootlet breakage (Avinash et al., 1993; Engström et al., 1983; Tilney et al., 1982). Generally speaking, mild stereocilia changes are associated with temporary threshold shift-inducing noise exposure, whereas severe stereocilia damage is associated with PTS-inducing noise exposure (Liberman, 1987; Liberman and Dodds, 1987). Consistent with the potential role of FCHSD2 in stereocilia maintenance, we found that *Fchsd2* knockout mice show increased vulnerability to acoustic stimuli.

Journal of Cell Science (2022) 135, jcs259912. doi:10.1242/jcs.259912

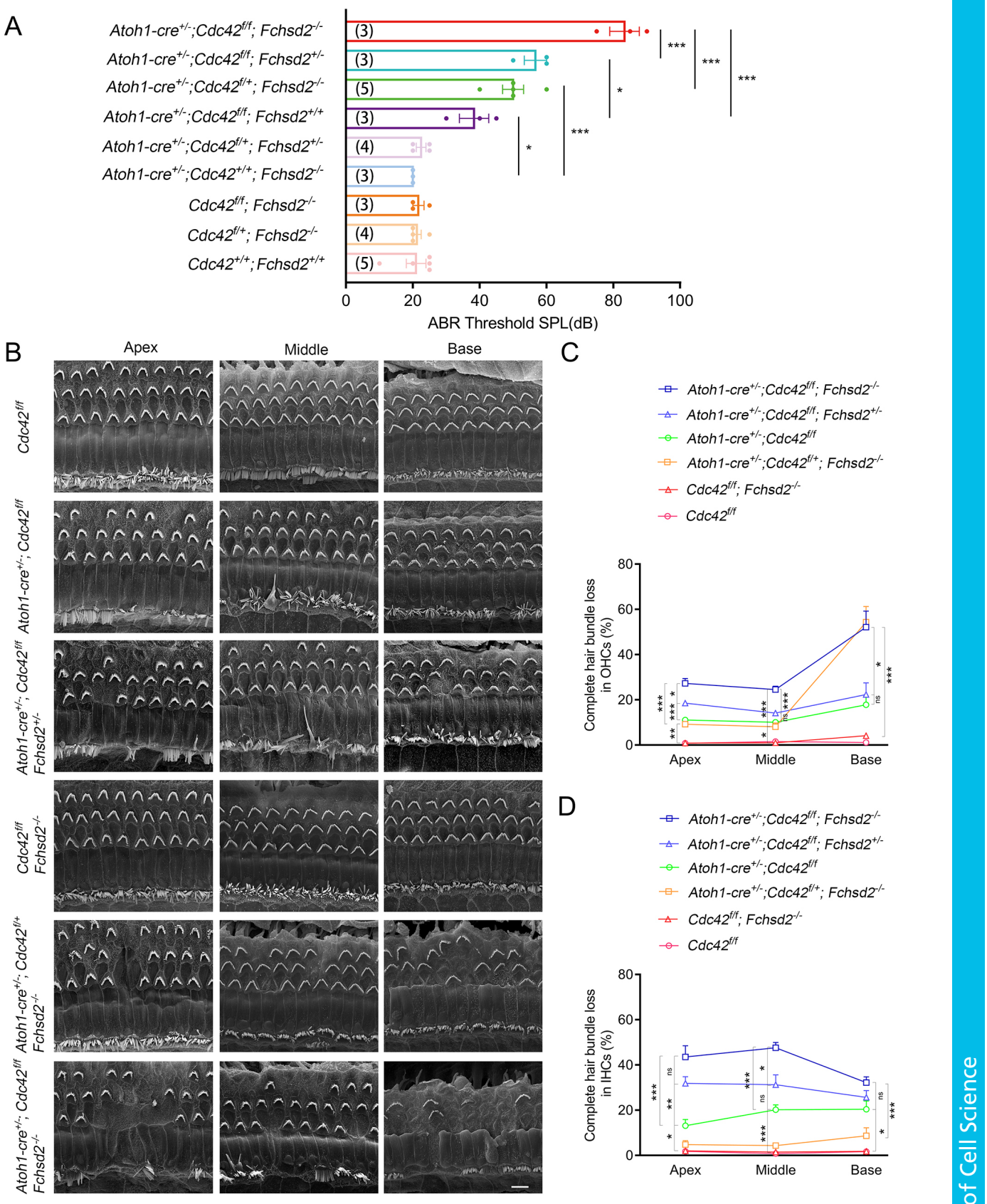

Fig. 6. FCHSD2 and CDC42 cooperate to regulate auditory function and stereocilia maintenance in mice. (A) ABR thresholds to click stimuli in 1-month-old mice of the indicated genotypes. *Cdc42*$^{f/f}$ indicates *Cdc42*$^{loxP/loxP}$. Data are presented as mean±s.e.m. The numbers of animals used for each genotype are indicated in brackets. (B) SEM images of cochlear hair bundles at the indicated positions in 1-month-old mice of different genotypes. Scale bar: 5 µm. (C) Percentage of complete OHC hair bundle loss, calculated using images as shown in B. (D) Percentage of complete IHC hair bundle loss, calculated using images as shown in B. Data in C and D are presented as mean+s.e.m., and three mice were used for each genotype. **P*<0.05; ***P*<0.01; ****P*<0.001; ns, not significant (one-way ANOVA with Tukey's test in A; one-way ANOVA with Dunnett's test in C,D).

Journal of Cell Science

Journal of Cell Science (2022) 135, jcs259912. doi:10.1242/jcs.259912

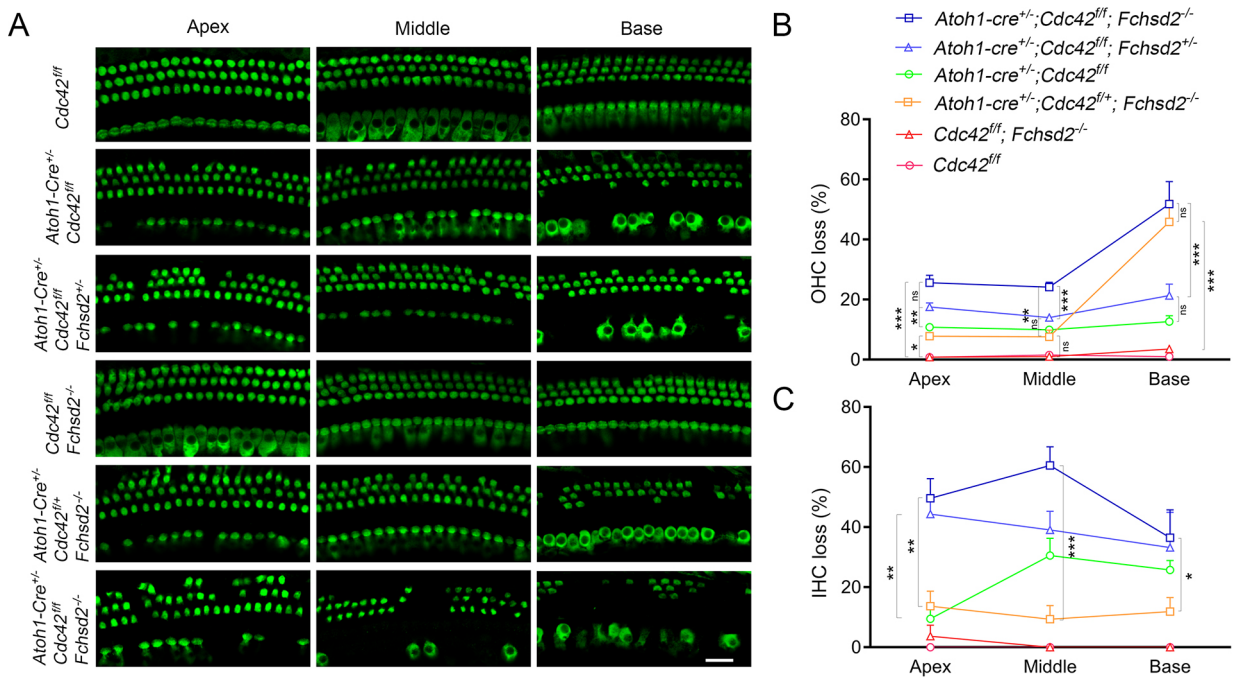

Fig. 7. Hair cell loss is enhanced in *Cdc42*/*Fchsd2* double knockout mice. (A) Whole-mount immunostaining was performed using an anti-MYO7A antibody to label hair cells at the apical (apex), middle and basal (base) turns of cochleae from 1-month-old mice of the indicated genotypes. *Cdc42*$^{f/f}$ denotes *Cdc42*$^{loxP/loxP}$. Single confocal images are shown. Scale bar: 10 µm. (B) Percentage of OHC loss, quantified using images as shown in A. (C) Percentage of IHC loss, quantified using images as shown in A. Data in B and C are presented as mean+s.e.m., and three mice were used in each group. **P*<0.05; ***P*<0.01; ****P*<0.001; ns, not significant (one-way ANOVA with Dunnett's test).

Upon the same acoustic stimuli, *Fchsd2* knockout mice developed more severe PTS compared with that of control mice. Further examination revealed that noise exposure induced temporary IHC ribbon synapse loss in both *Fchsd2* knockout and control mice, whereas noise exposure caused OHC stereocilia degeneration as well as permanent OHC loss in *Fchsd2* knockout mice only. These results suggest that *Fchsd2* knockout mice show increased OHC stereocilia degeneration and more profound PTS upon acoustic stimulation, further supporting an important role of FCHSD2 in stereocilia maintenance. Interestingly, besides the third-row stereocilia, the tallest first-row stereocilia in *Fchsd2*$^{-/-}$ OHCs also degenerated after acoustic stimulation. First-row stereocilia degeneration has been reported in OHCs deficient for the TRIOBP-5 isoform of TRIOBP, which localizes at the stereocilia rootlet (Katsuno et al., 2019). Whether FCHSD2 plays a role in stereocilia rootlet awaits further investigation.

As a BAR protein, FCHSD2 contains a N-terminal BAR domain, two SH3 domains and a C-terminal PDZ domain-binding interface (PBI). The BAR domain of FCHSD2 mediates protein dimerization as well as plasma membrane binding, while SH3 domains interact with other proteins such as ITSN1, WASP and N-WASP (Almeida-Souza et al., 2018; Cao et al., 2013). The PBI of FCHSD2 interacts with PDZ domain-containing proteins such as MAGI-1 and CASK (Ohno et al., 2003). Recently, we have shown that FCHSD2 and CDC42 simultaneously bind to N-WASP and cooperatively regulate actin-based cell protrusion formation in COS-7 cells (Zhai et al., 2022). Here, our results suggest that FCHSD2 and CDC42 may also cooperatively regulate stereocilia maintenance in mouse cochlear hair cells. CDC42 has been shown to localize along the hair cell stereocilia, and *Cdc42* knockout affects stereocilia development and maintenance in mice (Du et al., 2021; Kirjavainen et al., 2015; Ueyama et al., 2014). Our present data show that simultaneous knockout of *Fchsd2* and *Cdc42* causes more severe stereocilia degeneration as well as more profound hearing loss in mice, suggesting that they may work together to regulate stereocilia maintenance.

FCHSD2 and CDC42 act on the same downstream target proteins – WASP or N-WASP – to regulate ARP2/3-dependent F-actin assembly and cell protrusion formation (Alekhina et al., 2017; Zhai et al., 2022). Proteomic screening studies have revealed the existence of several ARP2/3 subunits in the stereocilia, although their precise localization remains unknown (Krey et al., 2015; Shin et al., 2013). WASP and N-WASP have not been detected in the stereocilia, but low levels of mRNA expression in the hair cells have been reported in the gEAR and SHIELD database (Orvis et al., 2021; Shen et al., 2015). It is noteworthy that the stereocilia are based on unbranched, parallel F-actin, whereas WASP and N-WASP usually activate ARP2/3 and mediate branched F-actin polymerization (Alekhina et al., 2017). Therefore, whether FCHSD2 and CDC42 regulate stereocilia maintenance through WASP or N-WASP and ARP2/3 awaits further investigation. Alternatively, our data reveal that FCHSD2 immunoreactivity is localized at the perimeter of the stereociliary F-actin core and inside the plasma membrane. Therefore, FCHSD2 might regulate stereocilia stability by bridging between the stereociliary F-actin core and the plasma membrane through its C-terminal domains and its N-terminal BAR domain, respectively.

Our data show that stereocilia morphology in *Fchsd2* knockout mice is largely normal until 2 months of age and that only OHCs are affected by *Fchsd2* knockout, suggesting that other proteins might compensate for the loss of FCHSD2 in *Fchsd2* knockout mice to some extent. A good candidate is FCHSD1, the homolog of FCHSD2, which is also expressed in the auditory hair cells (Cao et al., 2013). Although FCHSD1 has lower binding affinity toward WASP and N-WASP when compared with that of FCHSD2, it can efficiently stimulate WASP–ARP2/3-mediated F-actin

Journal of Cell Science (2022) 135, jcs259912. doi:10.1242/jcs.259912

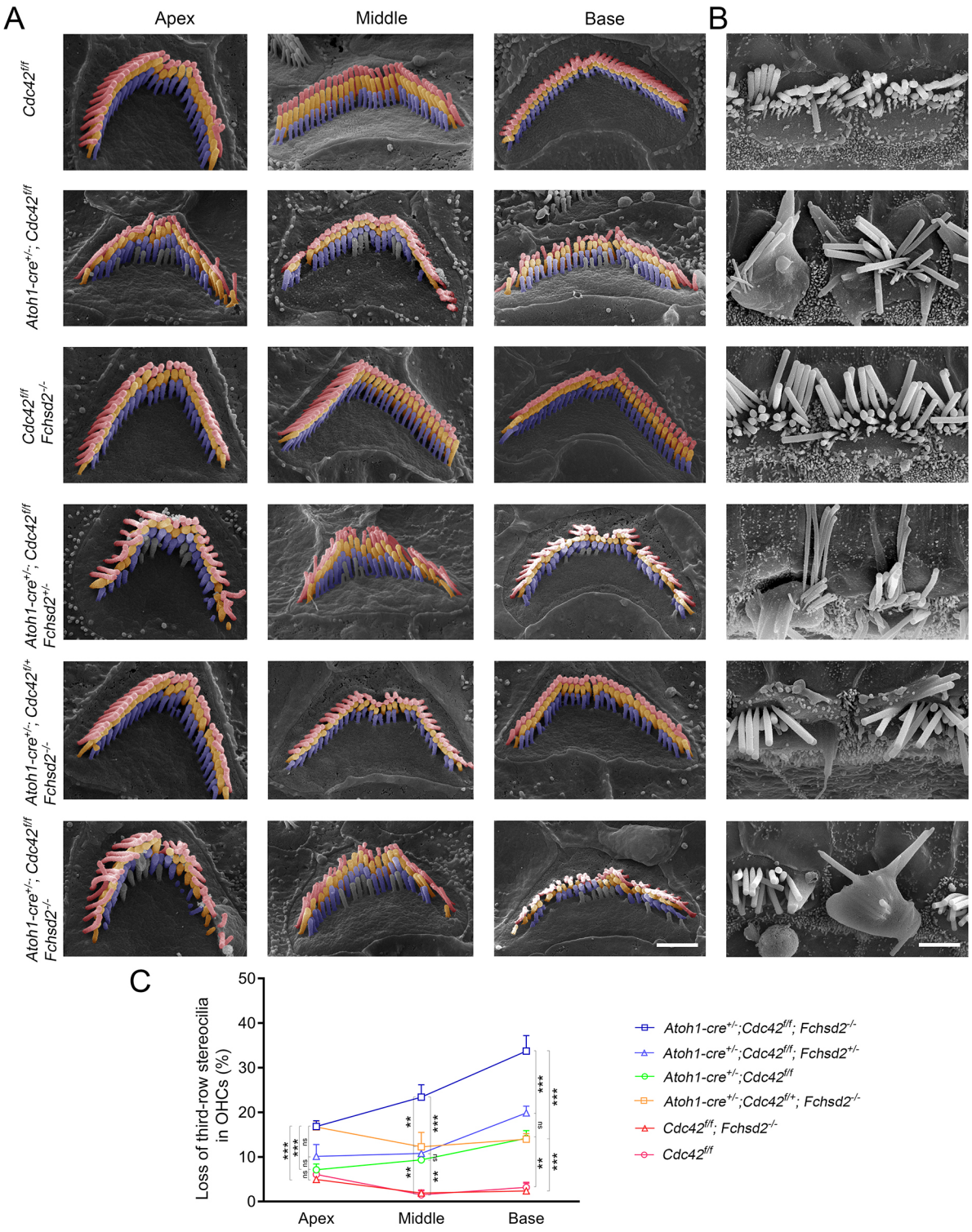

Fig. 8. FCHSD2 and CDC42 cooperate to regulate stereocilia maintenance in mice. (A) Higher magnification SEM images of cochlear OHC hair bundles at the apical (apex), middle and basal (base) turns in 1-month-old mice of the indicated genotypes (*Cdc42*$^{f/f}$ denotes *Cdc42*$^{loxP/loxP}$). First-row stereocilia are shown in red; second-row stereocilia are shown in yellow; third-row stereocilia are shown in violet. Scale bar: 1 µm. (B) Higher magnification SEM images of cochlear IHC hair bundles at middle turn in 1-month-old mice as indicated in A. Scale bar: 2 µm. (C) Percentage of loss of third-row stereocilia in OHCs, calculated using images as shown in A. Data are presented as mean+s.e.m. For each group, at least 20 cells from three mice were analyzed. ***P*<0.01; ****P*<0.001; ns, not significant (one-way ANOVA with Dunnett's test).

polymerization through binding to sorting nexin 9 (SNX9) (Cao et al., 2013). *Fchsd1*/*Fchsd2* double knockout mice would certainly help us to learn more about the mechanism of how FCHSD1 and FCHSD2 regulate stereocilia development and/or maintenance.

MATERIALS AND METHODS

Animals

Animal experiments were approved by the Animal Ethics Committee of Shandong University School of Life Sciences (permit number SYDWLL-

Journal of Cell Science (2022) 135, jcs259912. doi:10.1242/jcs.259912

2017-05) and were performed accordingly. *Fchsd2*$^{loxP/+}$ mice in C57BL/6 background were generated by Shanghai Biomodel Organism Science & Technology Development Co., Ltd. Briefly, a targeting vector was constructed to insert two *loxP* sites flanking exon 2 of the mouse *Fchsd2* gene. Mouse *Pgk1* promoter-driven neomycin resistance gene and herpes simplex virus thymidine kinase gene were included for positive and negative selection, respectively. The targeting vector was electroporated into embryonic stem cells (ESCs), and G418 and ganciclovir double-resistant colonies were screened by performing genotyping PCR (Fchsd2-F1, 5′-CAGTCTCATGGACTTCCTTTTTGGC-3′; Neo-R1, 5′-GGCCTACC-CGCTTCCATTGCTC-3′; Neo-F2, 5′-TCGCATTGTCTGAGTAGGTG-TC-3′; Fchsd2-R2, 5′-AAGGGAAAGAGGGAGGAAAGGAACCA-3′). Homologous recombinant ESCs were microinjected into C57BL/6 female mice to obtain heterozygous *Fchsd2*$^{loxP/+}$ mice, which were then crossed with *EIIa-Cre* transgenic mice (Lakso et al., 1996) in a mixed background to eventually obtain *Fchsd2*$^{-/-}$ mice.

Fchsd2$^{+/\Delta 37}$ mice in C57BL/6 background were generated using the CRISPR/Cas9 genome editing technique by Shanghai Biomodel Organism Science & Technology Development Co., Ltd. Briefly, three small guide RNAs (sgRNAs) that target different sites were *in vitro* transcribed (site-1, 5′-CAAGAGCTGAGAAACATTCAAGG-3′; site-2, 5′-AAAACTTCAA-GCCAAACATCAGG-3′; site-3, 5′-GTCACATTCTGCCTGATGTTTGG-3′) in exon 2 of the mouse *Fchsd2* gene. The sgRNAs were mixed with *Cas9* mRNA and injected into the cytoplasm of C57BL/6J zygotes. After culturing *in vitro* for 24 h, the injected zygotes were transferred into the oviduct of a pseudopregnant ICR female mouse at 0.5 days post coitus (dpc) to give rise to F0 mice. To determine the sequences of mutant alleles, F0 mice were examined by performing genotyping PCR (Fchsd2-F, 5′-GGTCTTTGGGGATAGGAAAAC-3′; Fchsd2-R, 5′-CAGATACA-GAAGTTCTCCAGC-3′) and Sanger sequencing. F0 mice were crossed with C57BL/6J mice to obtain F1 *Fchsd2*$^{+/\Delta 37}$ mice. *Fchsd2*$^{+/\Delta 37}$ mice were then crossed with wild-type mice in a mixed background, and the offspring were used for the functional studies.

Atoh1-Cre$^{+/-}$; *Cdc42*$^{loxP/loxP}$ mice were obtained by crossing *Cdc42*$^{loxP/+}$ mice (van Hengel et al., 2008; Wu et al., 2006) in C57BL/6 background with *Atoh1-Cre*$^{+/-}$ mice in a mixed background that express Cre recombinase under the control of *Atoh1* promoter (Yang et al., 2010).

Antibodies and other reagents

Rabbit anti-FCHSD2 polyclonal antibody was developed by Abmart (Shanghai, China). Briefly, mouse FCHSD2 (1–631 amino acids) was expressed as GST fusion protein in *Escherichia coli* and purified using Glutathione Sepharose 4B (GE Healthcare), as described previously (Cao et al., 2013). The fusion protein was then used to immunize two rabbits, and IgG was purified using Protein A agarose affinity chromatography. The dilutions used in immunostaining and western blotting were 1:200 and 1:1000, respectively. Prestained protein molecular mass marker was purchased from Thermo Fisher Scientific (cat. no. 26612). Mouse anti-GAPDH polyclonal antibody was purchased from Millipore (cat. no. MAB374; 1:5000 dilution for western blotting). Rabbit anti-MYO7A polyclonal antibody was purchased from Proteus Biosciences (cat. no. 25-6790; 1:400 dilution for immunostaining). Mouse anti-CtBP2 antibody (IgG1) was purchased from BD (cat. no. 612044; 1:400 dilution for immunostaining). Mouse anti-GluR2 antibody (IgG2a) was purchased from Millipore (cat. no. MAB397; 1:1000 dilution for immunostaining). Alexa Fluor 488-conjugated donkey anti-rabbit IgG secondary antibody was purchased from Thermo Fisher Scientific (cat. no. A21206; 1:400 dilution for immunostaining). Alexa Fluor 568-conjugated goat anti-mouse IgG1 was purchased from Invitrogen (cat. no. A21124; 1:400 dilution for immunostaining). Alexa Fluor 488-conjugated goat anti-mouse IgG2a was purchased from Invitrogen (cat. no. A21131; 1:400 dilution for immunostaining). HRP-conjugated goat anti-rabbit IgG secondary antibody was purchased from Bio-Rad (cat. no. 170-6515; 1:3000 dilution for western blotting). HRP-conjugated goat anti-mouse IgG secondary antibody was purchased from Bio-Rad (cat. no. 170-6516; 1:5000 dilution for western blotting). TRITC-conjugated phalloidin was purchased from Sigma-Aldrich (cat. no. P1951; 1:1000 dilution for staining). SF488-conjugated phalloidin was purchased from Solarbio (cat. no. CA1640; 1:1000 dilution for staining). DAPI was purchased from Gene View Scientific Inc. (cat. no. GD3408; 1:3000 dilution for staining).

Western blotting and whole-mount immunostaining

For western blotting, dissected tissues or cells were homogenized and lysed in ice-cold RIPA buffer (Beyotime, P0013B) with 1 mM PMSF and 1× protease inhibitor cocktail (Roche). After centrifugation, the supernatant was collected and separated by polyacrylamide gel electrophoresis (PAGE), then transferred to PVDF membrane. After blocking in TBS (20 mM Tris-HCl, 150 mM NaCl) containing 5% non-fat dry milk and 0.05% Tween-20, the membrane was incubated with primary antibody at 4°C overnight, followed by incubation with HRP-conjugated secondary antibody at room temperature for 1 h. The signals were detected with the ECL system (Thermo Fisher Scientific) (Fig. S6).

For whole-mount immunostaining, organ of Corti explants were dissected and fixed with 4% paraformaldehyde (PFA) in PBS for 30 min, followed by permeabilization with 0.5% Triton X-100 for 20 min and blocking with 5% donkey serum (Solarbio, cat. no. SL050) for 1 h at room temperature. For FCHSD2 staining, the samples were additionally incubated in 10% methanol for 15 min at −20°C before permeabilization. Samples were then incubated with primary antibody in PBS overnight at 4°C, and with secondary antibody in PBS for 1 h at room temperature. For stereocilia visualization, samples were incubated with phalloidin in PBS for 30 min at room temperature. For nuclei visualization, samples were incubated with DAPI in PBS for 1 h at room temperature. For CtBP2 and GluR2 staining, samples were incubated with primary and secondary antibodies at 37°C overnight or for 1 h, respectively. Afterwards, samples were mounted in PBS and glycerol (1:1 mixture) and imaged with a confocal microscope (LSM 700 or 880, Zeiss, Germany) with a 1.25 NA/Apo 63× M27 or 1.4 NA/Apo 100× M27 objective. OHCs and IHCs were counted along successive 0.2 mm intervals at different cochlear turns by a second person blind to the experimental conditions. A hair cell was considered as missing if MYO7A immunoreactivity or the phalloidin and DAPI signals were absent.

Auditory brainstem response measurement

ABR measurement was performed as described previously (Du et al., 2020). Stimulus generation, presentation, ABR acquisition and data management were achieved using a RZ6 workstation and BioSig software (Tucker Davis Technologies, Inc.). Mice were anesthetized by intraperitoneal injection of pentobarbital (8.4 mg/100 g body weight). The electrodes were then put subcutaneously at the vertex, the pinna and near the tail. Acoustic stimuli (clicks or pure-tone bursts) of sound level decreasing from 90 dB SPL in 10 dB SPL steps were delivered to the mouse ear through an earphone. Hearing threshold was indicated by the lowest sound level at which all ABR waves were detectable.

Scanning electron microscopy

Mouse temporal bones were dissected and fixed with 2.5% glutaraldehyde in 0.1 M phosphate buffer at 4°C overnight. The cochleae were dissected out of the temporal bone and post-fixed with 1% osmium tetroxide in 0.1 M phosphate buffer at 4°C for 2 h. The samples were dehydrated in ethanol, then underwent critical point drying using a Leica EM CPD300 (Leica, Germany), followed by mounting and sputter coating with platinum (15 nm) using a Cressington 108 sputter coater (Cressington, UK). The samples were imaged with a Quanta250 field-emission scanning electron microscope (FEI, The Netherlands). Hair bundle numbers were counted along successive 0.2 mm intervals at different cochlear turns by a second person blind to the experimental conditions. To quantify the loss of first- or third-row stereocilia, the stereocilia numbers in each row from individual OHCs were counted by a second person blind to the experimental conditions. The percentage of first- or third-row stereocilia loss was calculated by subtracting the number of first- or third-row stereocilia from the number of second-row stereocilia, then dividing the resulting value by the number of second-row stereocilia before multiplying by 100. Stereocilia length measurement was performed as previously described (Li et al., 2020). Briefly, SEM images were taken in two imaging planes of different angles. The relative stereocilia projection length and angles in the reconstructed three-dimensional

coordinates were measured using Photoshop (Adobe). The stereocilia length was then calculated using equations described previously (Li et al., 2020).

Noise exposure

Mice were located in a sound-exposure chamber with loudspeakers driven by a power amplifier (AWA5870B; Aihua Instruments Co., Hangzhou, China). Audio sound files were created and equalized using audio editing software (AWA6290M; Aihua Instruments Co.). Sound levels were calibrated using a sound level meter (AWA6221A; Aihua Instruments Co.) at multiple locations within the chamber. Mice of different genotypes were exposed to 2–20 kHz noise at 106 dB SPL for 2 h, and then put back in their home cage. ABR thresholds were measured before exposure and at different post-exposure time points. At certain time points, some of the mice were euthanized, and the stereocilia and ribbon synapses were examined by performing SEM and immunostaining.

Statistical analysis

The numbers of independent animals are indicated in the figure legends. Data are shown as mean±s.e.m. Appropriate tests used to determine statistical significance are indicated in the figure legends.

Acknowledgements

We thank Sen Wang, Xiaomin Zhao and Haiyan Yu from the core facilities for Life and Environmental Sciences, Shandong University, for technical support in SEM and confocal microscopy.

Competing interests

The authors declare no competing or financial interests.

Author contributions

Conceptualization: Z.X.; Methodology: X. Zhai, H.D., Y.S., X. Zhang, Z.C., Y.W.; Formal analysis: X. Zhai, Z.X.; Investigation: X. Zhai, H.D., Y.S., X. Zhang, Y.W.; Resources: Z.C.; Writing - original draft: Z.X.; Supervision: Z.X.; Funding acquisition: Y.W., Z.X.

Funding

This work was supported by grants from the National Natural Science Foundation of China (82192861, 82071051, 31401007 and 31070969) and the Natural Science Foundation of Shandong Province (ZR2020ZD39 and ZR2020QC098).

References

Alekhina, O., Burstein, E. and Billadeau, D. D. (2017). Cellular functions of WASP family proteins at a glance. *J. Cell Sci.* **130**, 2235-2241. doi:10.1242/jcs.199570

Almeida-Souza, L., Frank, R. A. W., García-Nafría, J., Colussi, A., Gunawardana, N., Johnson, C. M., Yu, M., Howard, G., Andrews, B., Vallis, Y. et al. (2018). A flat BAR protein promotes actin polymerization at the base of clathrin-coated pits. *Cell* **174**, 325-337.e14. doi:10.1016/j.cell.2018.05.020

Avinash, G. B., Nuttall, A. L. and Raphael, Y. (1993). 3-D analysis of F-actin in stereocilia of cochlear hair cells after loud noise exposure. *Hear. Res.* **67**, 139-146. doi:10.1016/0378-5955(93)90241-R

Barr-Gillespie, P.-G. (2015). Assembly of hair bundles, an amazing problem for cell biology. *Mol. Biol. Cell* **26**, 2727-2732. doi:10.1091/mbc.E14-04-0940

Becalska, A. N., Kelley, C. F., Berciu, C., Stanishneva-Konovalova, T. B., Fu, X., Wang, S. Y., Sokolova, O. S., Nicastro, D. and Rodal, A. A. (2013). Formation of membrane ridges and scallops by the F-BAR protein Nervous Wreck. *Mol. Biol. Cell* **24**, 2406-2418. doi:10.1091/mbc.e13-05-0271

Beurg, M., Fettiplace, R., Nam, J.-H. and Ricci, A. J. (2009). Localization of inner hair cell mechanotransducer channels using high-speed calcium imaging. *Nat. Neurosci.* **12**, 553-558. doi:10.1038/nn.2295

Cao, H., Yin, X., Cao, Y., Jin, Y., Wang, S., Kong, Y., Chen, Y., Gao, J., Heller, S. and Xu, Z. (2013). FCHSD1 and FCHSD2 are expressed in hair cell stereocilia and cuticular plate and regulate actin polymerization in vitro. *PLoS ONE* **8**, e56516. doi:10.1371/journal.pone.0056516

Carlson, B. and Soderling, S. H. (2009). Mechanisms of cellular protrusions branch out. *Dev. Cell* **17**, 307-309. doi:10.1016/j.devcel.2009.08.015

Carlson, B. R., Lloyd, K. E., Kruszewski, A., Kim, I.-H., Rodriguiz, R. M., Heindel, C., Faytell, M., Dudek, S. M., Wetsel, W. C. and Soderling, S. H. (2011). WRP/srGAP3 facilitates the initiation of spine development by an inverse F-BAR domain, and its loss impairs long-term memory. *J. Neurosci.* **31**, 2447-2460. doi:10.1523/JNEUROSCI.4433-10.2011

Carlton, A. J., Halford, J., Underhill, A., Jeng, J. Y., Avenarius, M. R., Gilbert, M. L., Ceriani, F., Ebisine, K., Brown, S. D. M., Bowl, M. R. et al. (2021). Loss of Baiap2l2 destabilizes the transducing stereocilia of cochlear hair cells and leads to deafness. *J. Physiol.* **599**, 1173-1198. doi:10.1113/JP280670

Carman, P. J. and Dominguez, R. (2018). BAR domain proteins-a linkage between cellular membranes, signaling pathways, and the actin cytoskeleton. *Biophys. Rev.* **10**, 1587-1604. doi:10.1007/s12551-018-0467-7

Chen, F.-Q., Zheng, H.-W., Hill, K. and Sha, S.-H. (2012). Traumatic noise activates Rho-family GTPases through transient cellular energy depletion. *J. Neurosci.* **32**, 12421-12430. doi:10.1523/JNEUROSCI.6381-11.2012

Coutinho-Budd, J., Ghukasyan, V., Zylka, M. J. and Polleux, F. (2012). The F-BAR domains from srGAP1, srGAP2 and srGAP3 regulate membrane deformation differently. *J. Cell Sci.* **125**, 3390-3401. doi:10.1242/jcs.098962

Drummond, M. C., Barzik, M., Bird, J. E., Zhang, D.-S., Lechene, C. P., Corey, D. P., Cunningham, L. L. and Friedman, T. B. (2015). Live-cell imaging of actin dynamics reveals mechanisms of stereocilia length regulation in the inner ear. *Nat. Commun.* **6**, 6873. doi:10.1038/ncomms7873

Du, H., Zou, L., Ren, R., Li, N., Li, J., Wang, Y., Sun, J., Yang, J., Xiong, W. and Xu, Z. (2020). Lack of PDZD7 long isoform disrupts ankle-link complex and causes hearing loss in mice. *FASEB J.* **34**, 1136-1149. doi:10.1096/fj.201901657RR

Du, H., Zhou, H., Sun, Y., Zhai, X., Chen, Z., Wang, Y. and Xu, Z. (2021). The Rho GTPase cell division cycle 42 regulates stereocilia development in cochlear hair cells. *Front. Cell Dev. Biol.* **9**, 765559. doi:10.3389/fcell.2021.765559

Engström, B., Flock, A. and Borg, E. (1983). Ultrastructural studies of stereocilia in noise-exposed rabbits. *Hear. Res.* **12**, 251-264. doi:10.1016/0378-5955(83)90110-7

Fang, Q., Indzhykulian, A. A., Mustapha, M., Riordan, G. P., Dolan, D. F., Friedman, T. B., Belyantseva, I. A., Frolenkov, G. I., Camper, S. A. and Bird, J. E. (2015). The 133-kDa N-terminal domain enables myosin 15 to maintain mechanotransducing stereocilia and is essential for hearing. *Elife* **4**, e08627. doi:10.7554/eLife.08627

Fettiplace, R. (2017). Hair cell transduction, tuning, and synaptic transmission in the mammalian cochlea. *Compr. Physiol.* **7**, 1197-1227. doi:10.1002/cphy.c160049

Flock, A. and Cheung, H. C. (1977). Actin filaments in sensory hairs of inner ear receptor cells. *J. Cell Biol.* **75**, 339-343. doi:10.1083/jcb.75.2.339

Furness, D. N., Johnson, S. L., Manor, U., Rüttiger, L., Tocchetti, A., Offenhauser, N., Olt, J., Goodyear, R. J., Vijayakumar, S., Dai, Y. et al. (2013). Progressive hearing loss and gradual deterioration of sensory hair bundles in the ears of mice lacking the actin-binding protein Eps8L2. *Proc. Natl. Acad. Sci. USA* **110**, 13898-13903. doi:10.1073/pnas.1304644110

Gillespie, P. G. and Müller, U. (2009). Mechanotransduction by hair cells: models, molecules, and mechanisms. *Cell* **139**, 33-44. doi:10.1016/j.cell.2009.09.010

Gong, T.-W., Fairfield, D. A., Fullarton, L., Dolan, D. F., Altschuler, R. A., Kohrman, D. C. and Lomax, M. I. (2012). Induction of heat shock proteins by hyperthermia and noise overstimulation in hsf1$^{-/-}$ mice. *J. Assoc. Res. Otolaryngol.* **13**, 29-37. doi:10.1007/s10162-011-0289-9

Guerrier, S., Coutinho-Budd, J., Sassa, T., Gresset, A., Jordan, N. V., Chen, K., Jin, W.-L., Frost, A. and Polleux, F. (2009). The F-BAR domain of srGAP2 induces membrane protrusions required for neuronal migration and morphogenesis. *Cell* **138**, 990-1004. doi:10.1016/j.cell.2009.06.047

Hasson, T., Gillespie, P. G., Garcia, J. A., MacDonald, R. B., Zhao, Y., Yee, A. G., Mooseker, M. S. and Corey, D. P. (1997). Unconventional myosins in inner-ear sensory epithelia. *J. Cell Biol.* **137**, 1287-1307. doi:10.1083/jcb.137.6.1287

Hudspeth, A. J. and Jacobs, R. (1979). Stereocilia mediate transduction in vertebrate hair cells. *Proc. Natl. Acad. Sci. USA* **76**, 1506-1509. doi:10.1073/pnas.76.3.1506

Jones, C., Roper, V. C., Foucher, I., Qian, D., Banizs, B., Petit, C., Yoder, B. K. and Chen, P. (2008). Ciliary proteins link basal body polarization to planar cell polarity regulation. *Nat. Genet.* **40**, 69-77. doi:10.1038/ng.2007.54

Kalinec, F., Zhang, M., Urrutia, R. and Kalinec, G. (2000). Rho GTPases mediate the regulation of cochlear outer hair cell motility by acetylcholine. *J. Biol. Chem.* **275**, 28000-28005. doi:10.1074/jbc.M004917200

Katsuno, T., Belyantseva, I. A., Cartagena-Rivera, A. X., Ohta, K., Crump, S. M., Petralia, R. S., Ono, K., Tona, R., Imtiaz, A., Rehman, A. et al. (2019). TRIOBP-5 sculpts stereocilia rootlets and stiffens supporting cells enabling hearing. *JCI Insight* **4**, e128561. doi:10.1172/jci.insight.128561

Kazmierczak, M., Kazmierczak, P., Peng, A. W., Harris, S. L., Shah, P., Puel, J.-L., Lenoir, M., Franco, S. J. and Schwander, M. (2017). Pejvakin, a candidate stereociliary rootlet protein, regulates hair cell function in a cell-autonomous manner. *J. Neurosci.* **37**, 3447-3464. doi:10.1523/JNEUROSCI.2711-16.2017

Kelley, C. F., Messelaar, E. M., Eskin, T. L., Wang, S., Song, K., Vishnia, K., Becalska, A. N., Shupliakov, O., Hagan, M. F., Danino, D. et al. (2015). Membrane charge directs the outcome of F-BAR domain lipid binding and autoregulation. *Cell Rep.* **13**, 2597-2609. doi:10.1016/j.celrep.2015.11.044

Kirjavainen, A., Laos, M., Anttonen, T. and Pirvola, U. (2015). The Rho GTPase Cdc42 regulates hair cell planar polarity and cellular patterning in the developing cochlea. *Biol. Open* **4**, 516-526. doi:10.1242/bio.20149753

Kitajiri, S., Sakamoto, T., Belyantseva, I. A., Goodyear, R. J., Stepanyan, R., Fujiwara, I., Bird, J. E., Riazuddin, S., Riazuddin, S., Ahmed, Z. M. et al. (2010). Actin-bundling protein TRIOBP forms resilient rootlets of hair cell stereocilia essential for hearing. *Cell* **141**, 786-798. doi:10.1016/j.cell.2010.03.049

Kobel, M., Le Prell, C. G., Liu, J., Hawks, J. W. and Bao, J. (2017). Noise-induced cochlear synaptopathy: past findings and future studies. *Hear. Res.* **349**, 148-154. doi:10.1016/j.heares.2016.12.008

Krey, J. F. and Barr-Gillespie, P. G. (2019). Molecular composition of vestibular hair bundles. *Cold Spring Harb. Perspect. Med.* **9**, a033209. doi:10.1101/cshperspect.a033209

Krey, J. F., Sherman, N. E., Jeffery, E. D., Choi, D. and Barr-Gillespie, P. G. (2015). The proteome of mouse vestibular hair bundles over development. *Sci. Data* **2**, 150047. doi:10.1038/sdata.2015.47

Krey, J. F., Krystofiak, E. S., Dumont, R. A., Vijayakumar, S., Choi, D., Rivero, F., Kachar, B., Jones, S. M. and Barr-Gillespie, P. G. (2016). Plastin 1 widens stereocilia by transforming actin filament packing from hexagonal to liquid. *J. Cell Biol.* **215**, 467-482. doi:10.1083/jcb.201606036

Krey, J. F., Chatterjee, P., Dumont, R. A., O'Sullivan, M., Choi, D., Bird, J. E. and Barr-Gillespie, P. G. (2020). Mechanotransduction-dependent control of stereocilia dimensions and row identity in inner hair cells. *Curr. Biol.* **30**, 442-454.e7. doi:10.1016/j.cub.2019.11.076

Kujawa, S. G. and Liberman, M. C. (2009). Adding insult to injury: cochlear nerve degeneration after "temporary" noise-induced hearing loss. *J. Neurosci.* **29**, 14077-14085. doi:10.1523/JNEUROSCI.2845-09.2009

Lakso, M., Pichel, J. G., Gorman, J. R., Sauer, B., Okamoto, Y., Lee, E., Alt, F. W. and Westphal, H. (1996). Efficient in vivo manipulation of mouse genomic sequences at the zygote stage. *Proc. Natl. Acad. Sci. USA* **93**, 5860-5865. doi:10.1073/pnas.93.12.5860

Li, S. H., Mecca, A., Kim, J., Caprara, G. A., Wagner, E. L., Du, T.-T., Petrov, L., Xu, W. H., Cui, R. J., Rebustini, I. T. et al. (2020). Myosin-VIIa is expressed in multiple isoforms and essential for tensioning the hair cell mechanotransduction complex. *Nat. Commun.* **11**, 2066. doi:10.1038/s41467-020-15936-z

Liberman, M. C. (1987). Chronic ultrastructural changes in acoustic trauma: serial-section reconstruction of stereocilia and cuticular plates. *Hear. Res.* **26**, 65-88. doi:10.1016/0378-5955(87)90036-0

Liberman, M. C. (2017). Noise-induced and age-related hearing loss: new perspectives and potential therapies. *F1000Res* **6**, 927. doi:10.12688/f1000research.11310.1

Liberman, M. C. and Dodds, L. W. (1987). Acute ultrastructural changes in acoustic trauma: serial-section reconstruction of stereocilia and cuticular plates. *Hear. Res.* **26**, 45-64. doi:10.1016/0378-5955(87)90035-9

Liu, H. Z., Pecka, J. L., Zhang, Q., Soukup, G. A., Beisel, K. W. and He, D. Z. Z. (2014). Characterization of transcriptomes of cochlear inner and outer hair cells. *J. Neurosci.* **34**, 11085-11095. doi:10.1523/JNEUROSCI.1690-14.2014

Maoileidigh, D. O. and Ricci, A. J. (2019). A bundle of mechanisms: Inner-ear hair-cell mechanotransduction. *Trends Neurosci.* **42**, 221-236. doi:10.1016/j.tins.2018.12.006

Miyoshi, T., Belyantseva, I. A., Kitajiri, S.-I., Miyajima, H., Nishio, S.-Y., Usami, S.-I., Kim, B. J., Choi, B. Y., Omori, K., Shroff, H. et al. (2021). Human deafness-associated variants alter the dynamics of key molecules in hair cell stereocilia F-actin cores. *Hum. Genet.* **141**, 363-382. doi:10.1007/s00439-021-02304-0

Narayanan, P., Chatterton, P., Ikeda, A., Ikeda, S., Corey, D. P., Ervasti, J. M. and Perrin, B. J. (2015). Length regulation of mechanosensitive stereocilia depends on very slow actin dynamics and filament-severing proteins. *Nat. Commun.* **6**, 6855. doi:10.1038/ncomms7855

Nayak, G. D., Ratnayaka, H. S. K., Goodyear, R. J. and Richardson, G. P. (2007). Development of the hair bundle and mechanotransduction. *Int. J. Dev. Biol.* **51**, 597-608. doi:10.1387/ijdb.072392gn

Ohno, H., Hirabayashi, S., Kansaku, A., Yao, I., Tajima, M., Nishimura, W., Ohnishi, H., Mashima, H., Fujita, T., Omata, M. et al. (2003). Carom: a novel membrane-associated guanylate kinase-interacting protein with two SH3 domains. *Oncogene* **22**, 8422-8431. doi:10.1038/sj.onc.1206996

Orvis, J., Gottfried, B., Kancherla, J., Adkins, R. S., Song, Y., Dror, A. A., Olley, D., Rose, K., Chrysostomou, E., Kelly, M. C. et al. (2021). gEAR: Gene Expression Analysis Resource portal for community-driven, multi-omic data exploration. *Nat. Methods* **18**, 843-844. doi:10.1038/s41592-021-01200-9

Peter, B. J., Kent, H. M., Mills, I. G., Vallis, Y., Butler, P. J. G., Evans, P. R. and McMahon, H. T. (2004). BAR domains as sensors of membrane curvature: The amphiphysin BAR structure. *Science* **303**, 495-499. doi:10.1126/science.1092586

Rodal, A. A., Motola-Barnes, R. N. and Littleton, J. T. (2008). Nervous wreck and Cdc42 cooperate to regulate endocytic actin assembly during synaptic growth. *J. Neurosci.* **28**, 8316-8325. doi:10.1523/JNEUROSCI.2304-08.2008

Rohatgi, R., Ma, L., Miki, H., Lopez, M., Kirchhausen, T., Takenawa, T. and Kirschner, M. W. (1999). The interaction between N-WASP and the Arp2/3 complex links Cdc42-dependent signals to actin assembly. *Cell* **97**, 221-231. doi:10.1016/S0092-8674(00)80732-1

Salzer, U., Kostan, J. and Djinović-Carugo, K. (2017). Deciphering the BAR code of membrane modulators. *Cell. Mol. Life Sci.* **74**, 2413-2438. doi:10.1007/s00018-017-2478-0

Scheffer, D. I., Shen, J., Corey, D. P. and Chen, Z.-Y. (2015). Gene expression by mouse inner ear hair cells during development. *J. Neurosci.* **35**, 6366-6380. doi:10.1523/JNEUROSCI.5126-14.2015

Shen, J., Scheffer, D. I., Kwan, K. Y. and Corey, D. P. (2015). SHIELD: an integrative gene expression database for inner ear research. *Database (Oxford)* **2015**, bav071. doi:10.1093/database/bav071

Shin, J.-B., Longo-Guess, C. M., Gagnon, L. H., Saylor, K. W., Dumont, R. A., Spinelli, K. J., Pagana, J. M., Wilmarth, P. A., David, L. L., Gillespie, P. G. et al. (2010). The R109H variant of Fascin-2, a developmentally regulated actin crosslinker in hair-cell stereocilia, underlies early-onset hearing loss of DBA/2J mice. *J. Neurosci.* **30**, 9683-9694. doi:10.1523/JNEUROSCI.1541-10.2010

Shin, J.-B., Krey, J. F., Hassan, A., Metlagel, Z., Tauscher, A. N., Pagana, J. M., Sherman, N. E., Jeffery, E. D., Spinelli, K. J., Zhao, H. et al. (2013). Molecular architecture of the chick vestibular hair bundle. *Nat. Neurosci.* **16**, 365-374. doi:10.1038/nn.3312

Simunovic, M., Evergren, E., Callan-Jones, A. and Bassereau, P. (2019). Curving cells inside and out: Roles of BAR domain proteins in membrane shaping and its cellular implications. *Annu. Rev. Cell Dev. Biol.* **35**, 111-129. doi:10.1146/annurev-cellbio-100617-060558

Taylor, R., Bullen, A., Johnson, S. L., Grimm-Günter, E.-M., Rivero, F., Marcotti, W., Forge, A. and Daudet, N. (2015). Absence of plastin 1 causes abnormal maintenance of hair cell stereocilia and a moderate form of hearing loss in mice. *Hum. Mol. Genet.* **24**, 37-49. doi:10.1093/hmg/ddu417

Tilney, L. G., Derosier, D. J. and Mulroy, M. J. (1980). The organization of actin filaments in the stereocilia of cochlear hair cells. *J. Cell Biol.* **86**, 244-259. doi:10.1083/jcb.86.1.244

Tilney, L. G., Saunders, J. C., Egelman, E. and DeRosier, D. J. (1982). Changes in the organization of actin filaments in the stereocilia of noise-damaged lizard cochleae. *Hear. Res.* **7**, 181-197. doi:10.1016/0378-5955(82)90013-2

Tilney, L. G., Tilney, M. S. and DeRosier, D. J. (1992). Actin filaments, stereocilia, and hair cells: how cells count and measure. *Annu. Rev. Cell Biol.* **8**, 257-274. doi:10.1146/annurev.cb.08.110192.001353

Ueyama, T., Sakaguchi, H., Nakamura, T., Goto, A., Morioka, S., Shimizu, A., Nakao, K., Hishikawa, Y., Ninoyu, Y., Kassai, H. et al. (2014). Maintenance of stereocilia and apical junctional complexes by Cdc42 in cochlear hair cells. *J. Cell Sci.* **127**, 2040-2052. doi:10.1242/jcs.143602

van Hengel, J., D'Hooge, P., Hooghe, B., Wu, X., Libbrecht, L., De Vos, R., Quondamatteo, F., Klempt, M., Brakebusch, C. and van Roy, F. (2008). Continuous cell injury promotes hepatic tumorigenesis in cdc42-deficient mouse liver. *Gastroenterology* **134**, 781-792. doi:10.1053/j.gastro.2008.01.002

Vélez-Ortega, A. C. and Frolenkov, G. I. (2019). Building and repairing the stereocilia cytoskeleton in mammalian auditory hair cells. *Hear. Res.* **376**, 47-57. doi:10.1016/j.heares.2018.12.012

Wu, X., Quondamatteo, F., Lefever, T., Czuchra, A., Meyer, H., Chrostek, A., Paus, R., Langbein, L. and Brakebusch, C. (2006). Cdc42 controls progenitor cell differentiation and β-catenin turnover in skin. *Genes. Dev.* **20**, 571-585. doi:10.1101/gad.361406

Yan, K. J., Zong, W., Du, H. B., Zhai, X. Y., Ren, R., Liu, S., Xiong, W., Wang, Y. F. and Xu, Z. G. (2022). BAIAP2L2 is required for the maintenance of mechanotransducing stereocilia of cochlear hair cells. *J. Cell. Physiol.* **237**, 774-788. doi:10.1002/jcp.30545

Yang, H., Xie, X., Deng, M., Chen, X. and Gan, L. (2010). Generation and characterization of Atoh1-Cre knock-in mouse line. *Genesis* **48**, 407-413. doi:10.1002/dvg.20633

Zhai, X., Shen, Y., Zhang, X., Li, T., Lu, Q. and Xu, Z. (2022). FCHSD2 cooperates with CDC42 and N-WASP to regulate cell protrusion formation. *Biochim. Biophys. Acta Mol. Cell Res.* **1869**, 119134. doi:10.1016/j.bbamcr.2021.119134

Zhang, D.-S., Piazza, V., Perrin, B. J., Rzadzinska, A. K., Poczatek, J. C., Wang, M., Prosser, H. M., Ervasti, J. M., Corey, D. P. and Lechene, C. P. (2012). Multi-isotope imaging mass spectrometry reveals slow protein turnover in hair-cell stereocilia. *Nature* **481**, 520-524. doi:10.1038/nature10745

Zheng, L. L., Sekerková, G., Vranich, K., Tilney, L. G., Mugnaini, E. and Bartles, J. R. (2000). The deaf jerker mouse has a mutation in the gene encoding the espin actin-bundling proteins of hair cell stereocilia and lacks espins. *Cell* **102**, 377-385. doi:10.1016/S0092-8674(00)00042-8

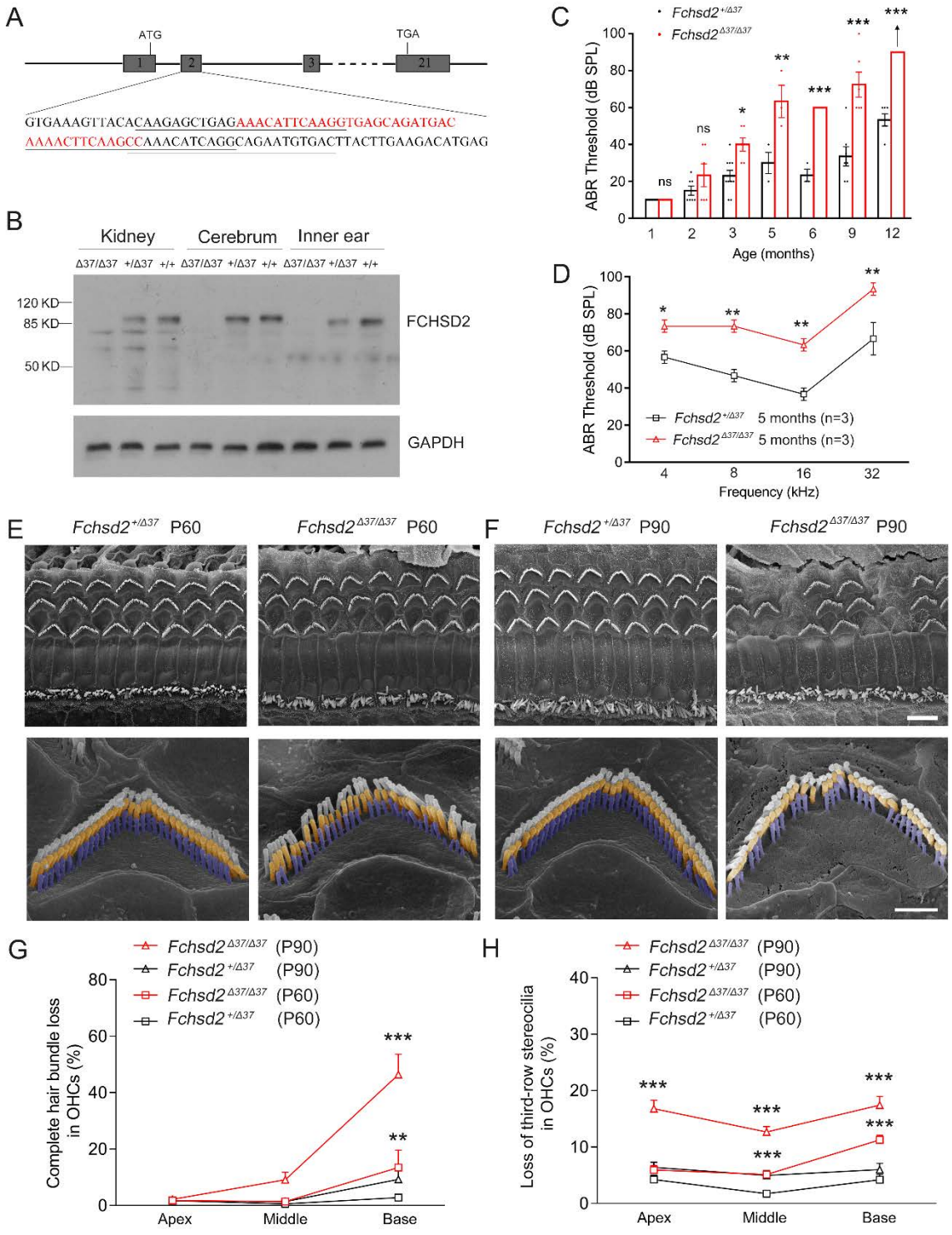

Fig. S1. *Fchsd2*$^{\Delta 37/\Delta 37}$ mice show progressive hearing loss as well as stereocilia maintenance deficits. (A) Schematic drawing of the strategy for constructing *Fchsd2*$^{\Delta 37/\Delta 37}$ mice. The target sites of CRISPR-Cas9 sgRNAs in the *Fchsd2* gene are

underlined. The deleted region in the genome of *Fchsd2*$^{\Delta 37/\Delta 37}$ mice is indicated in red. (B) Expression of FCHSD2 in various tissues from P8 mice of different genotypes was examined by performing western blotting using an anti-FCHSD2 antibody. GAPDH was used as internal control. (C) ABR thresholds to click stimuli in *Fchsd2*$^{+/\Delta 37}$ and *Fchsd2*$^{\Delta 37/\Delta 37}$ mice at different ages. Arrow indicates threshold above 90 dB SPL. Each dot represents an individual mouse. (D) ABR thresholds to pure tone stimuli in 5-month-old *Fchsd2*$^{+/\Delta 37}$ and *Fchsd2*$^{\Delta 37/\Delta 37}$ mice. Numbers of mice used in each group are indicated in brackets. (E) and (F) SEM images of hair bundles of *Fchsd2*$^{+/\Delta 37}$ and *Fchsd2*$^{\Delta 37/\Delta 37}$ mice at P60 (E) and P90 (F), respectively. Top panel, lower-magnification images of both OHCs and IHCs at the basal turn. Scale bar: 5 μm. Bottom panel, higher-magnification images of OHCs at the basal turn. Scale bar: 1 μm. The second-row stereocilia are indicated by yellow. The third-row stereocilia are indicated by violet. (G) Percentage of complete OHC hair bundle loss is calculated based on images shown in (E) and (F). (H) Percentages of third-row stereocilia loss in OHCs is calculated based on images shown in (E) and (F). For each group, at least 40 cells from at least three mice were analyzed. Data are presented as mean±s.e.m. *, $p<0.05$; **, $p<0.01$; ***, $p<0.001$ (one-way ANOVA with Tukey's test in C and D, one-way ANOVA with Dunnett's test in G and H).

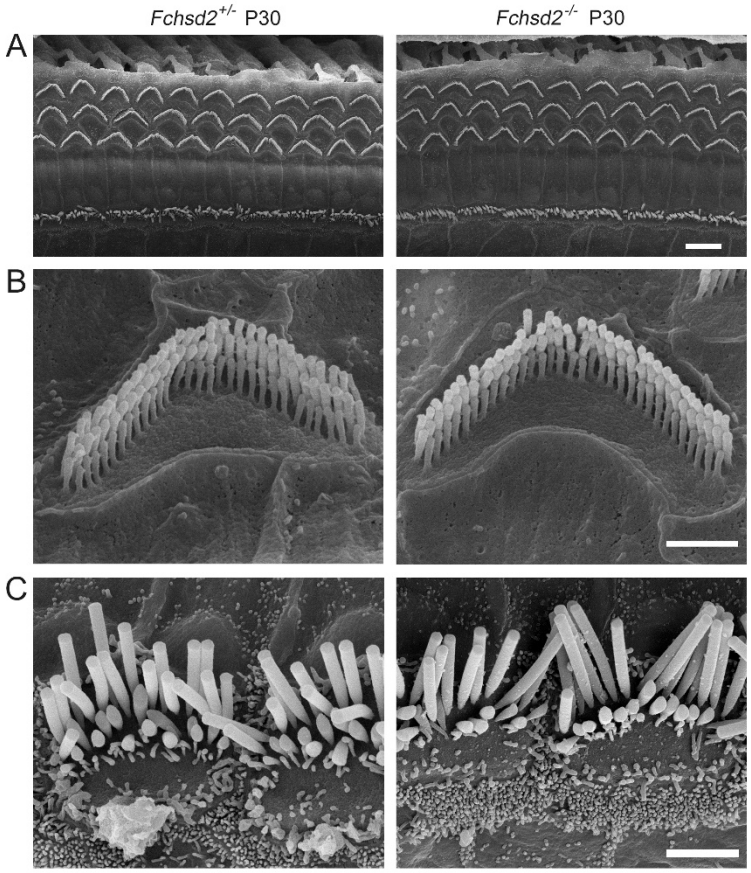

Fig. S2. Stereocilia morphology of *Fchsd2*$^{-/-}$ mice is largely normal by age of one month. (A) Low-magnification SEM images of cochlear hair bundles from 1-month-old *Fchsd2*$^{+/-}$ and *Fchsd2*$^{-/-}$ mice. (B) High-magnification SEM images of OHC bundles from 1-month-old *Fchsd2*$^{+/-}$ and *Fchsd2*$^{-/-}$ mice. (C) High-magnification SEM images of IHC bundles from 1-month-old *Fchsd2*$^{+/-}$ and *Fchsd2*$^{-/-}$ mice. Images were taken from the middle turn. Scale bars: 5 μm in (A), 1 μm in (B) and 2 μm in (C).

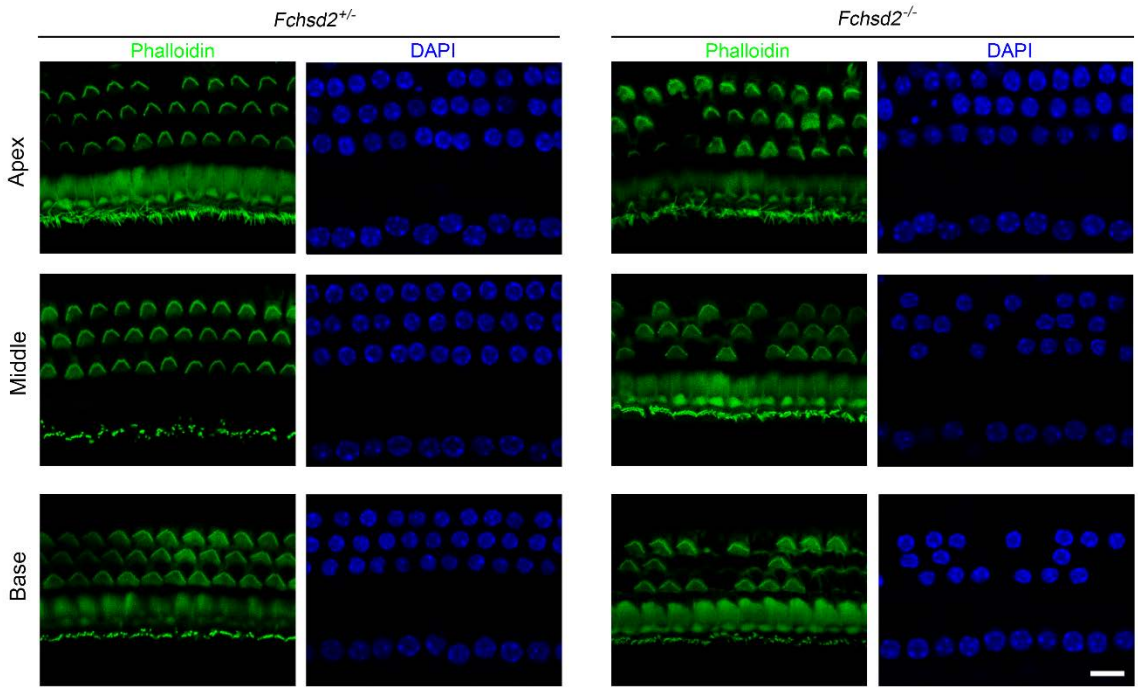

Fig. S3. OHC loss is increased in *Fchsd2*$^{-/-}$ mice when examined at 14 days after noise exposure. *Fchsd2*$^{+/-}$ mice or *Fchsd2*$^{-/-}$ mice at age of 1 month were exposed to 2-20 kHz noise at 106 dB SPL for 2 hours, and hair cells were examined by staining with SF488-conjugated phalloidin (green) and DAPI (blue). Scale bar: 5 μm.

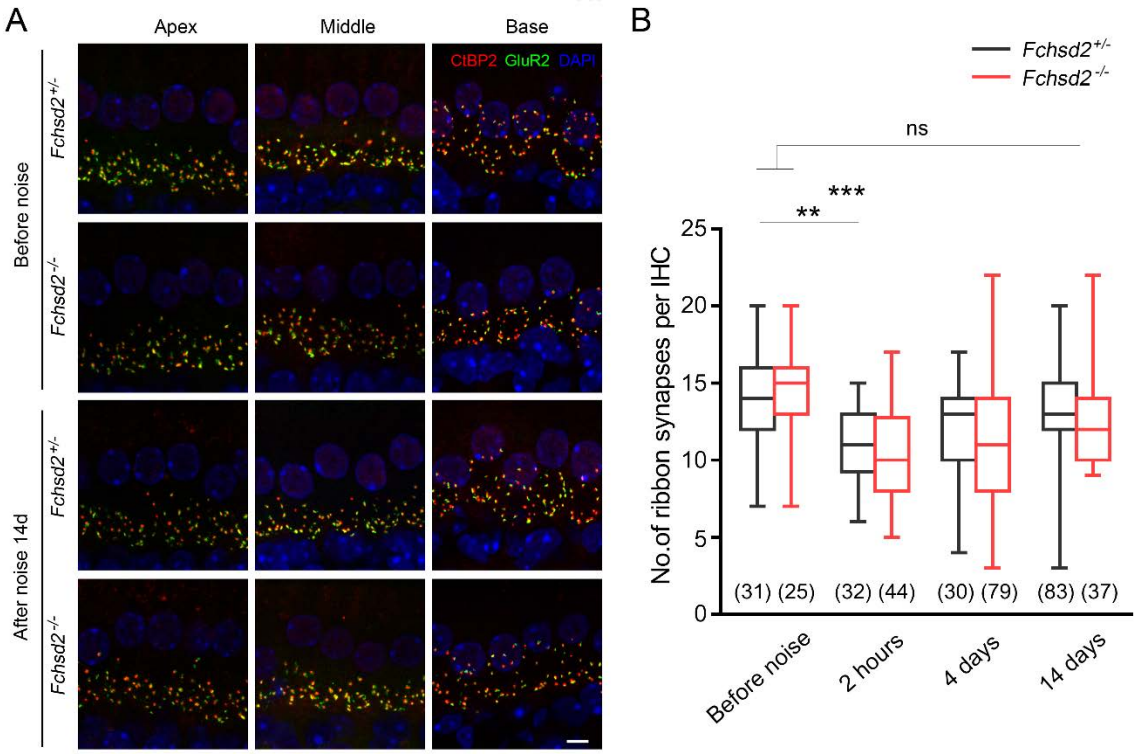

Fig. S4. Loss of ribbon synapses in *Fchsd2*$^{-/-}$ IHCs after noise exposure. (A) *Fchsd2*$^{+/-}$ mice and *Fchsd2*$^{-/-}$ mice at age of 1 month were exposed to 2-20 kHz noise at 106 dB SPL for 2 hours, and IHC ribbon synapses were examined by staining with an anti-CtBP2 antibody (red) and an anti-GluR2 antibody (green). Nuclei were visualized using DAPI (blue). Shown are images taken from the middle turns. Scale bar: 5 μm. (B) Double-possitive ribbon synapses were calculated based on the images shown in A. For each group, at least 20 cells from three mice were analyzed (cell numbers are indicated in brackets). Data are presented in box-and-whisker plots. ns, not significant; **, $p<0.01$; ***, $p<0.001$ (one-way ANOVA with Dunnett's test).

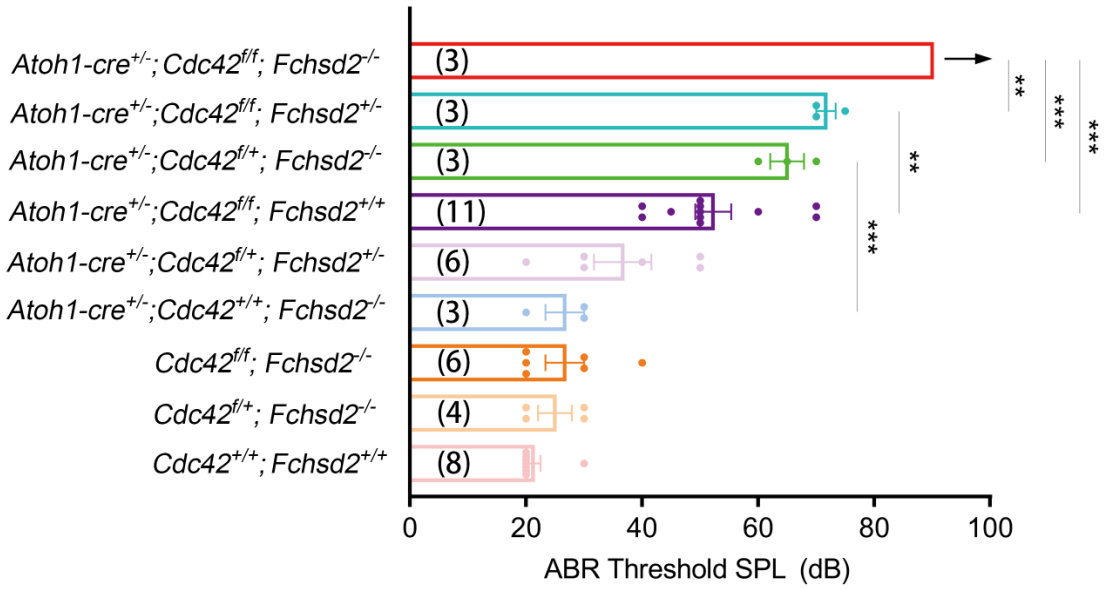

Fig. S5. *Fchsd2* and *Cdc42* knockout cooperatively affect auditory function in 2-month-old mice. Shown are ABR thresholds to click stimuli in 2-month-old mice of different genotypes. The numbers of animals used for each genotype are indicated in brackets. Data are presented as mean±s.e.m. **, $p<0.01$; ***, $p<0.001$ (one-way ANOVA with Tukey's test).

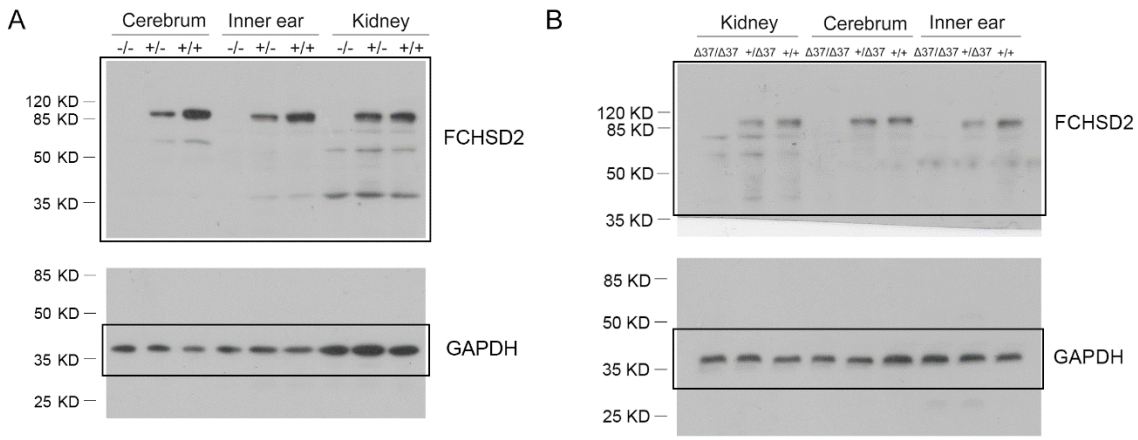

Fig. S6. Uncropped Western blots. (A) Uncropped blots corresponding to Fig. 1B. (B) Uncropped blots corresponding to Supplementary material Fig. S1B.